INL/EXT-13-28519

EBSD Characterization of Tubular Cladding Plasticity after Bend Testing: A Feasibility Study

Isabella J. van Rooyen

March 2013

The INL is a U.S. Department of Energy National Laboratory
operated by Battelle Energy Alliance

INL/EXT-13-28519

EBSD Characterization of Tubular Cladding Plasticity after Bend Testing: A Feasibility Study

Isabella J. van Rooyen

March 2013

Idaho National Laboratory
Idaho Falls, Idaho 83415

http://www.inl.gov

Prepared for the
U.S. Department of Energy
Office of Nuclear Energy
Under DOE Idaho Operations Office
Contract DE-AC07-05ID14517

EXECUTIVE SUMMARY

The Light Water Reactor Sustainability (LWRS) Program developed a bend test method for tubular samples during FY12. The purpose of this report is to provide details of the Electron Backscattered Diffraction (EBSD) measurements performed on the various sample sets to provide a comparative baseline of the impact that the silicon carbide ceramic matrix composites (SiC-CMC) sleeves had on the deformation and plasticity properties of the Zircaloy-4 (Zr-4) cladding tube.

A brief literature survey revealed no information on the effect of tubular bend test deformation on the EBSD texture analysis, although limited prior research was completed on beam (flat) samples. Specific deformation modes are not known under these conditions for tubular samples, nor are the influence of a specific sleeve or external clad on these deformation modes. Bend tests on tubular hybrid SiC-CMC Zr-4 samples were performed in FY12, but no specific prediction capability existed at Idaho National Laboratory (INL) to predict the performance of the CMC sleeves on the deformation of the inner Zr-4 cladding tube. This feasibility study was therefore undertaken to develop a powerful performance measurement tool for downstream selection of cladding designs.

The benefit of tomography as an indirect tool for establishing inputs for computational modeling tools such as localized deformation of the Zr-4 tube and SiC-CMC sleeve-Zr-4 cladding tube gap was clearly identified in this study. These measurements are considered valuable for the validation of the finite element analysis on deformation properties. An additional and significant benefit of these measurements as a non-destructive examination is that the specific levels and locations of deformation can be identified. The maximum deformation of 21% and 2% deformation are measured for the 2 ply- and 1 ply SiC-CMC hybrid Zr-4 sample respectively. This provided a good comparative deformation set for EBSD measurements.

The feasibility and value of EBSD measurements as deformation indicator on the Zr-4 tubes, has been demonstrated in this study. Comparative images and measurements were obtained from the Zr-4 cross sectional areas suggesting the texture changes on the Zr-4 tubes due to deformation, as well as demonstrating the different impact that different sleeve designs had. Although the data obtained in this study cannot be used as a quantitative measure yet, it provides the basis to show that differences are present and measureable, and therefore fulfill the objectives of this study.

Localized texture differences could be determined from this study between the baseline samples and the deformed samples. Compared to the baseline, non-deformed sample, localization and stronger 0001 texture development alongside the EBSD rolling direction (RD) direction are noticed for the deformed samples from the bend test. Interestingly, however, is that it is more prominent for the less deformed 1 ply SiC-CMC hybrid Zr-4 clad sample compared to the higher, 21% deformed 2 ply SiC-CMC hybrid Zr-4 clad sample. This is not fully understood yet. An alignment of grains parallel to the 2-1-10 transverse direction (TD) direction is also suggested for the bend samples. No significant changes were observed when comparing the pole figures from the annealed baseline with the un-annealed baseline samples. Although localized texture changes were observed, it would be interesting to include bulk texture analysis using X-ray diffraction (XRD) techniques. This can then provide a macro perspective on the deformation mechanisms.

This feasibility study additionally provides very valuable information on the sample preparation techniques and EBSD parameters needed for deformed Zircaloy material under these bend conditions. This will decrease preparation time for future similar work if pursued further.

It is recommended that a more detailed analysis be performed on the current data set for the finer nuances of structure and texture as affected by deformation. Re-analysis of the current data set can also be beneficial to identify possible twinning and the orientation of twin boundaries as a function of deformation level and SiC-CMC sleeve. For continuation, it is strongly recommended that more EBSD locations be included. This will provide a complete Zr-4 cross sectional thickness data set yielding

information on the transition point between compression and tensile stress areas at the point of maximum deflection. The finalization of the EBSD technique for hydrogen embrittlement identification is also strongly recommended. This necessitates the controlled hydrogen gas embrittlement studies with EBSD analyses to set a standard.

This work provides a solid baseline for future work as often the sample preparation is proven to be the most crucial part of the research, which was overcome in this study. Further incorporation of the potential measurements and deformation needs to be explored with the simulations group to identify the exact conditions and areas of measurements needed. For example, linkage of the sleeve-tube gap location and dimensions with heat transfer modeling studies and specific Zr-4 tube texture which may assist in failure mode determination and estimations.

ACKNOWLEDGEMENTS

Acknowledgements are given to the following persons:

- Tammy Trowbridge for EBSD data collection and sample preparation methods
- Todd Morris for EBSD microscopic sample preparation and optical microscopy
- Karen Wendt for 3D X-ray tomography measurements
- Arnold Erickson for the heat treatment of the baseline samples
- Amber Miller for assistance in sample coordination and heat treatment support
- Tom Lillo for the bench marking discussions on EBSD pole figure interpretations
- Brenda Monson and Connie Bates for administrative support
- Shannon Bragg-Sitton for the review of this report

CONTENTS

FIGURES

TABLES

ACRONYMS

ASTM	American Society for Testing and Materials
EBSD	Electron Backscattered Diffraction
EDMS	Engineering Document management System
EDS	energy dispersive spectroscopy
GTAW	Gas tungsten arc welding
IQ	Image quality
INL	Idaho National Laboratory
IPF	Inverse pole figure
LWR	Light Water Reactor
LWRS	Light water reactor sustainability
MOOSE	Multiphysics Object-Oriented Simulation Environment
N/A	Not applicable
PB	Parallel beam
PI	Principal Investigator
PIP	Polymer infiltration pyrolysis
QADP	Quality Assurance Program Document
RD	EBSD radial direction
SEM	Scanning electron microscopy
SiC-CMC	SiC ceramic matrix composites
TD	EBSD transverse rolling direction
XRD	X-ray diffraction
Zr-4	Zircaloy-4

EBSD Characterization of Tubular Cladding Plasticity after Bend Testing: A Feasibility Study

1. INTRODUCTION

Nuclear fuel performance is a significant driver of nuclear power plant operational performance, safety, economics and waste disposal requirements. The Advanced Light Water Reactor (LWR) Nuclear Fuel Development Pathway focuses on improving the scientific knowledge basis to enable the development of high-performance, high burn-up fuels with improved safety and cladding integrity and improved nuclear fuel cycle economics. To achieve significant improvements, fundamental changes are required in the areas of nuclear fuel composition, cladding integrity, and fuel/cladding interaction.

1.1 Background on the LWRS hybrid design

Selection of alternate cladding and structural materials must first take into account physical (geometric) and chemical compatibility with currently operating LWR designs. Several advanced cladding options under consideration focus on the use of silicon carbide (SiC). Both monolithic SiC and SiC composite have been studied by a variety of international research programs, resulting in a substantial body of data available to guide the current LWRS effort. Early research in the LWRS Fuels Pathway has focused on developing a better understanding of SiC ceramic matrix composites (SiC-CMC). Various candidate materials and designs are investigated, including both fully ceramic and "hybrid" designs. The hybrid concept would incorporate SiC as a structural material supplementing an inner metal tube (such as Zircaloy-4). Figure 1 shows the geometry of the LWRS capsule assembly design for the SiC-CMC hybrid Zr-4 cladding rodlet [1].

In addition to an appropriate level of mechanistic and systems-level modeling, significant out-of-pile testing is anticipated to fully characterize mechanical, physical and chemical properties of candidate materials and designs and to demonstrate performance under normal operating conditions and postulated accident conditions. Nonnuclear tests will provide a basis for initial down selection of candidate advanced cladding designs.

Advanced cladding materials must provide substantial benefit over the current zirconium-based cladding (e.g. Zircaloy-4, Zircaloy-2, ZIRLO and other). The planned tests are intended to either produce quantitative data or to demonstrate the properties required to achieve initial performance conditions relative to standard Zr-4 cladding:

1. Decreased hydrogen uptake (corrosion).
2. Decreased fretting of the cladding tube under normal operating and postulated accident conditions.
3. Increased coping time under postulated accident conditions (i.e. loss of coolant accident).
4. Reduced exothermic reaction rate with steam under postulated accident conditions (reduced hydrogen generation).
5. Possibility for power uprates and operation to higher burnup.

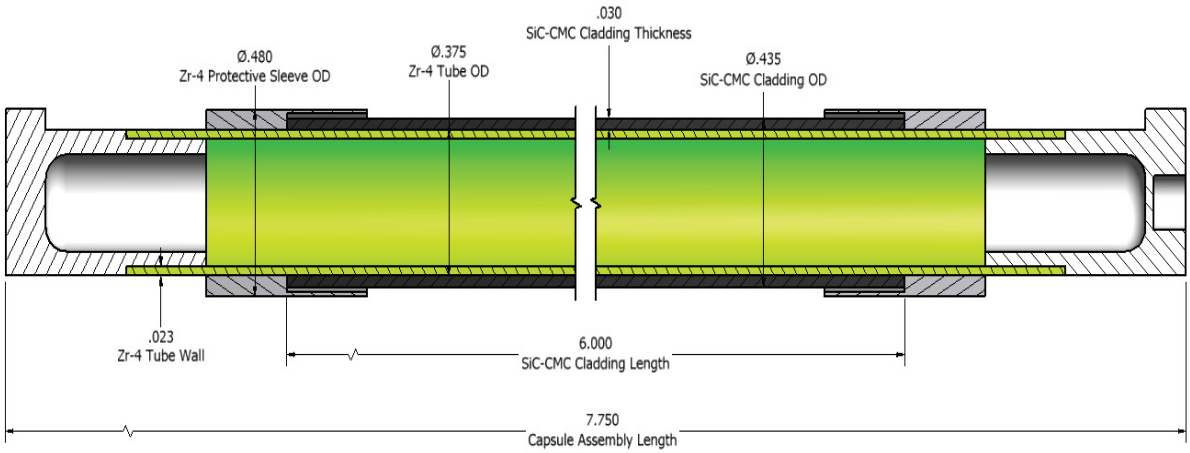

Figure 1. Geometry of the LWRS capsule assembly design for the Si-CMC hybrid Zr-4 cladding rodlet[1].

1.2 Scope of this study

The Light Water Reactor Sustainability (LWRS) Program developed a bend test method for tubular samples during FY12. The purpose of this report is to provide details of the Electron Backscattered Diffraction (EBSD) measurements performed on the various sample sets to provide a comparative baseline of the impact that the silicon carbide ceramic matrix composites (SiC-CMC) sleeves had on the deformation and plasticity properties of the Zircaloy-4 (Zr-4) cladding tube.

The purpose of this report is to provide the details of the EBSD measurements performed on the various sample sets to provide a comparative baseline of the impact of SiC-CMC sleeves on the deformation and plasticity properties of the Zr-4 cladding tube. Preliminary conclusions are drawn on the role of crystallographic texture on the deformation processes due to the tubular bend tests. Additionally, cross-sectional 3 D tomography images from the Zr-4 tube at various deflection points and baseline deformation measurements are presented to provide a rough indication of the amount of deformation experienced due to the bend test application.

Although ideally it is recommended to do these EBSD measurements at least at a few deflection positions, this study only provides a baseline for future recommendations on continuation and value of these measurements. Additionally, it is expected that this brief study will provide insight in the feasibility to use these integrated results as an input to future fuel performance modeling. Recommendations are also made regarding usefulness of EBSD measurements for determination and modeling of the deformation mechanisms. As the hybrid design is unique, limited to no information is available on the actual impact that a SiC CMC overbraid may have on the deformation and plasticity performance of the metallic cladding tube. If this method is demonstrated to reveal preliminary differences between the two different cladding systems, this may form a baseline for further exploration of EBSD measurements as a tool to obtain deformation mechanisms in alternate cladding tube designs.

The work scope is schematically shown in Figure 2. It needs to be noted that although some literature and recommendations are referenced and reported in this report, a detailed literature survey and full integration of this work were not possible at the limited funding level available.

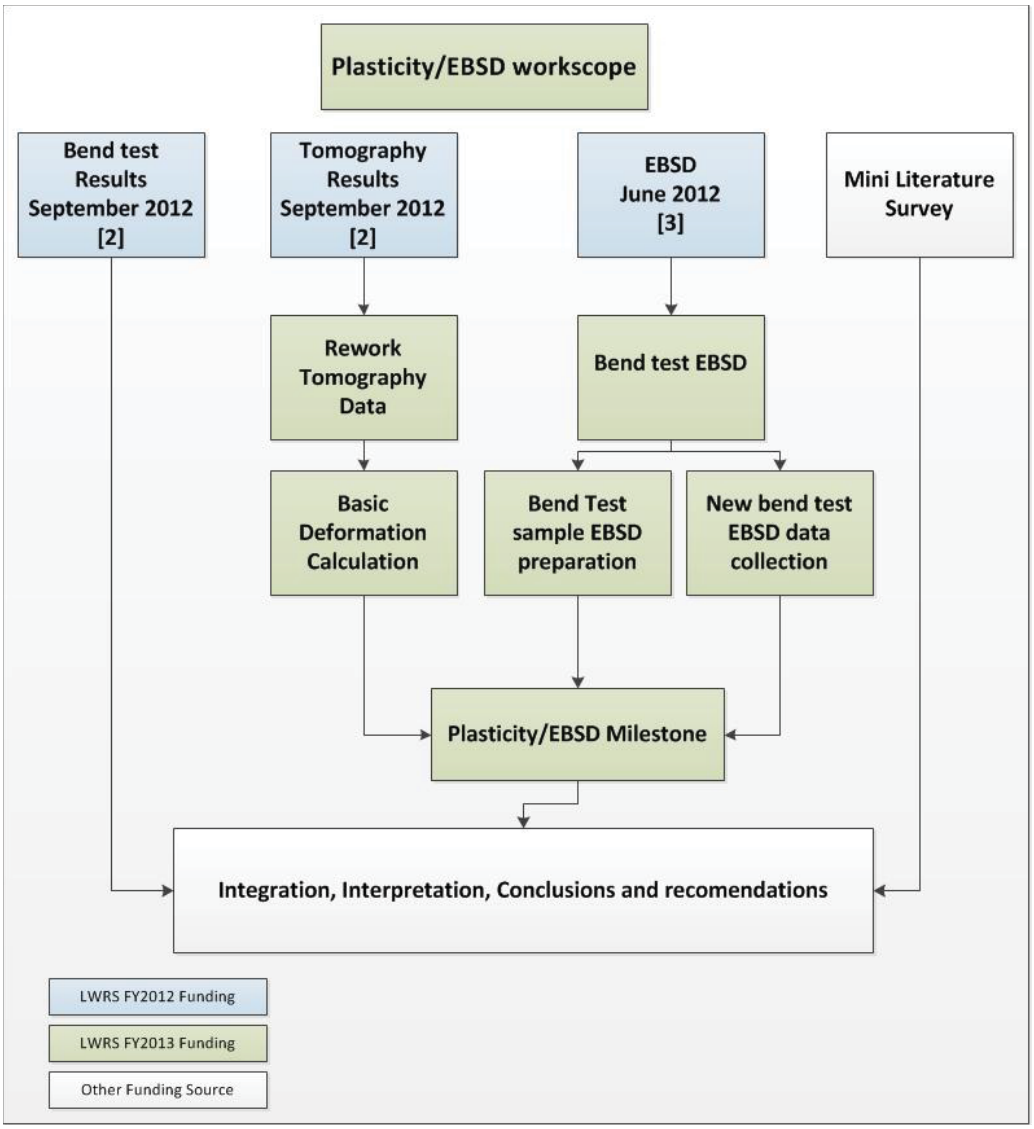

Figure 2. Schematic presentation of the work scope for this EBSD/Plasticity study on SiC-CMC-Zr-4 hybrid cladding after tubular bend testing.

1.3 Background on the role of crystallographic texture on deformation processes (plasticity)

Previous research performed on beam bend testing formed the basis of this specific feasibility study under the LWRS program. Kaschner *et al.* [4] provided information on the mechanical response of Zircaloy bent beams, showing the value of EBSD texture analysis as validation of the finite element analysis on beams. Their work demonstrated that the experimental results compared favorably with the predicted textures computed from a polycrystal plasticity code. Some questions remained, however, related to the hardening effect during deformation related to twinning.

Various other researchers completed more detailed studies on the lattice strain and texture evolution during deformation on Zirconium based alloys, but none are reported for tubular samples [5 - 13].

Kamaya also used EBSD to identify the local lattice strain gradient and subsequently measured the degree of local deformation. Kamaya further discussed the correlation between microstructural deformation and local grain misorientation in the zirconium alloy samples studied [6].

From the brief literature survey, no information was found on the effect of tubular bend test deformation on the localized macro- and micro- texture analysis. Specific deformation modes are not known under these conditions, nor are the influence of a specific sleeve or external clad on these deformation modes. Bend tests on tubular hybrid SiC-CMC Zr-4 samples were performed in FY12, but no specific prediction capability existed at INL to predict the performance of the CMC sleeves on the deformation of the inner Zr-4 cladding tube. This feasibility study was undertaken to develop a powerful performance measurement tool for downstream selection of cladding designs.

1.4 Summary of Bend Test Results on Mock-up Hybrid Samples [2]

Bend tests were completed in FY12 on 1 ply SiC-CMC hybrid mock-up tube, 2 ply hybrid SiC-CMC mock-up tube and a standard Zr-4 mock-up tube as part of a method development activity. This method covers the determination of a flexural strength test for a fully assembled hybrid tube at ambient temperature. Although the ASTM standard C1161-02c [14] is used as the basis for this four-point bend test, this test did not use rectangular standard test pieces. Alternately, testing was performed on the cylindrical experiment assembly with end cap fixtures to also test the end cap design. The bend test may show possible weaknesses in that area due to pulling out of the fibers on the end cap side. Furthermore, it is known that surface condition influences the flexural strength as well as the corrosion properties of the material. Using the actual experiment assembly ensures that the surface finish is fully representative of the as-fabricated condition. As it is not a standardized test, results are presented in comparison with the Zr-4 standard tube with end caps. Results of this four-point bend test will provide information on the robustness of the hybrid design. If this design is to be considered for future irradiation of fueled capsules, the established bend test method will also be required to support structural analysis of the SiC- CMC Zr-4 hybrid design to meet the intent of ASME Section III, Class 1 code [15].

The first test on the bare Zr-4 mock-up tube showed a shortfall in the initial test, as a maximum deflection value of 10% set on the Instron load cell prohibited the test to continue to a maximum load condition for Zr-4, as shown in Figure 3. This limit was corrected when the hybrid mock-up samples were tested. The deflectometer used in the test, shown in Figure 4, provided a more accurate measurement of the deflection up to 2% changes, allowing early detection of material changes. Additionally, the deflectometer provided verification for the built-in deflection measurement system of the Instron load cell. No differences between these two measurements were found for all three mock-up samples. (Graphs in Figure 4 show only the Instron measurements). Figures 4 to 6 show the bend test at the start and completion of all three mock-up samples. Slippage of the saddles was observed at the end of the testing of the hybrid mock up samples SiC-1 and SiC-2. This is not considered to have influenced the final results as the comparative nature of the test still showed sufficient differences between the bending momentum of the three samples. Figure 3 shows that the 2 ply SiC-CMC hybrid mock-up sample exhibited the highest bending moment while the Zr-4 mock-up sample exhibited the lowest. Cracking and bundling of the SiC-CMC fibers was observed for the 2 ply braided sleeve hybrid mock-up sample (SiC-1) in the mid section of maximum deflection, while no bundling or cracking was observed for the 1 ply braided hybrid mock-up sample (SiC-2).

It was concluded that the method development for both hybrid SiC-CMC-Zr-4 mock-up and bare SiC-CMC sleeve samples were successful for a comparative method. The 2 ply sleeve samples show a higher bend momentum compared to those of the 1 ply sleeve samples for both the hybrid mock-up and the bare SiC-CMC sleeve samples. Comparatively, both the 1 and 2 ply hybrid mock-up samples showed a higher bend momentum compared to the standard Zr-4 mock-up sample.

The characterization of the hybrid mock-up samples showed signs of distress and preliminary signs of defraying at the protective Zr-4 sleeve areas on the 1 ply SiC-CMC sleeve matrix. In addition, the microstructure of the SiC matrix at the cracks after bend test shows significant cracking and flaking. The 2 ply SiC-CMC sleeve samples revealed a well-bonded, cohesive SiC matrix structure. The observed cracking and fraying suggest potential concerns for increased fretting during the actual use of the hybrid designed cladding tubes.

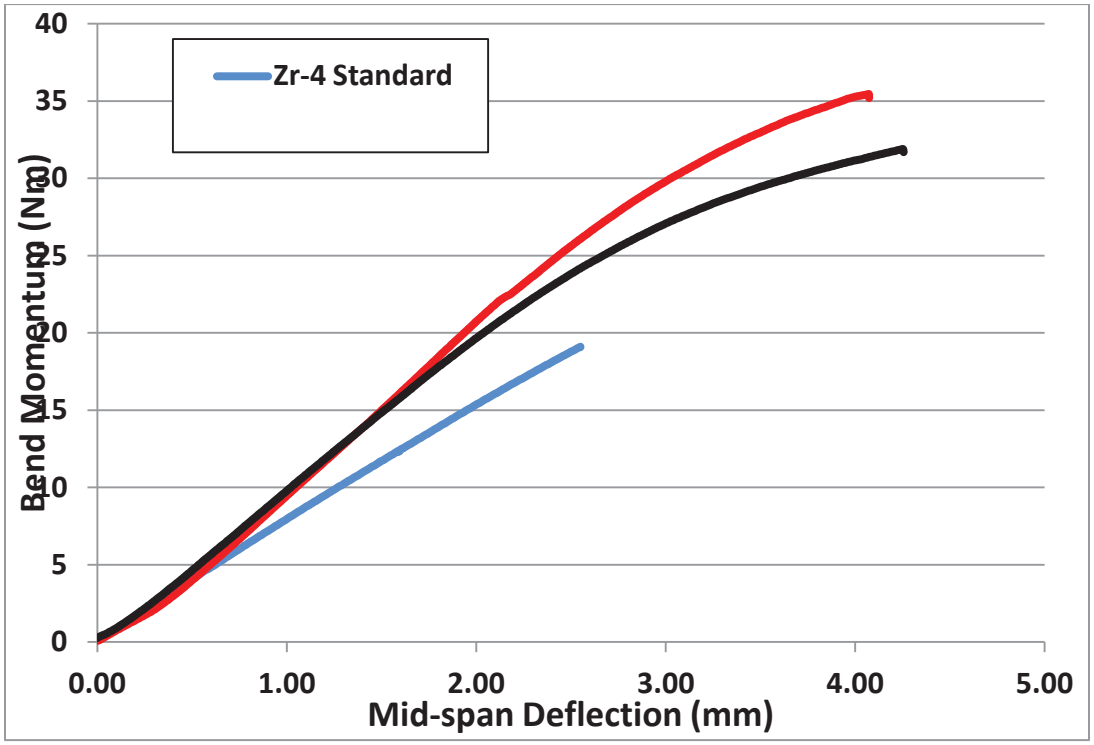

Figure 3. Bend test results of the mock-up samples showing bending momentum vs mid-span deflection. The 2 ply SiC-CMC hybrid mock-up sample exhibits the highest bend momentum.

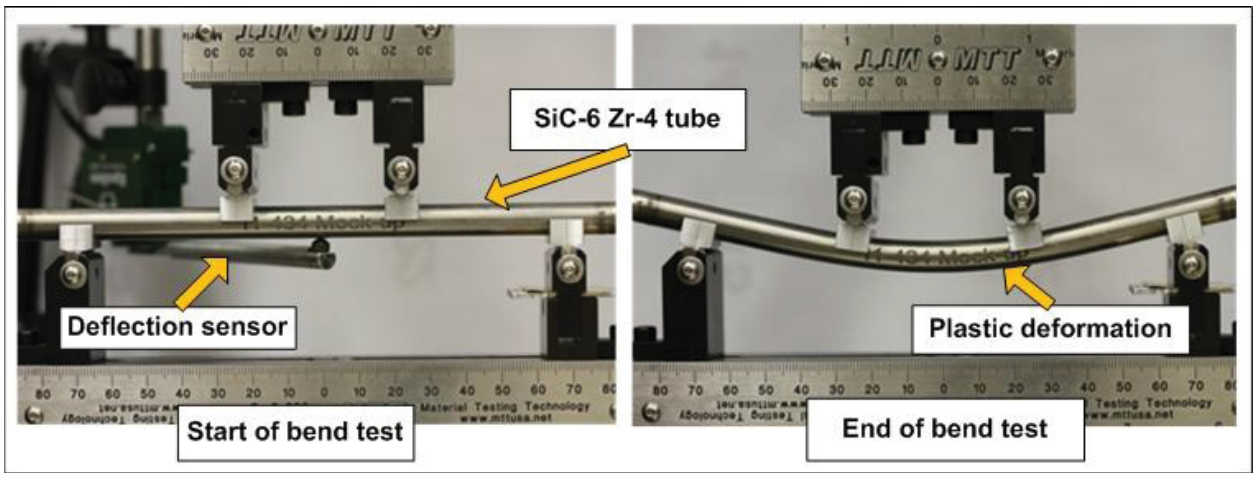

Figure 4. Bend test results of the Zr-4 mock-up sample (SiC-6) at start and end of bend test, showing plastic deformation.

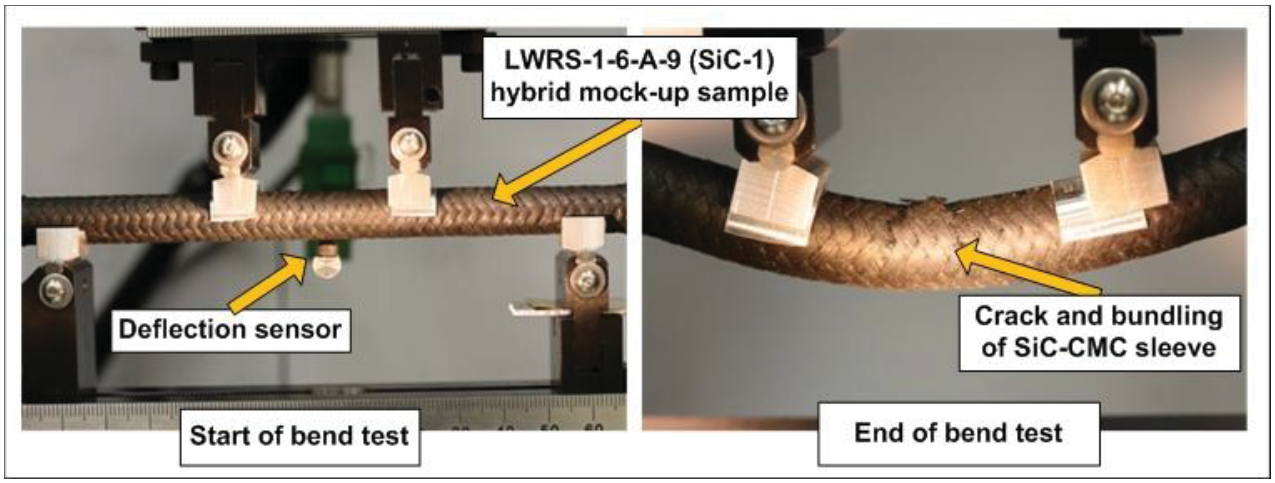

Figure 5. Bend test results of the 7 cycles, 2 ply LWRS-1-6-A-9 mock-up sample (SiC-1) at start and end of bend test, showing cracking and bundling of the SiC-CMC sleeve.

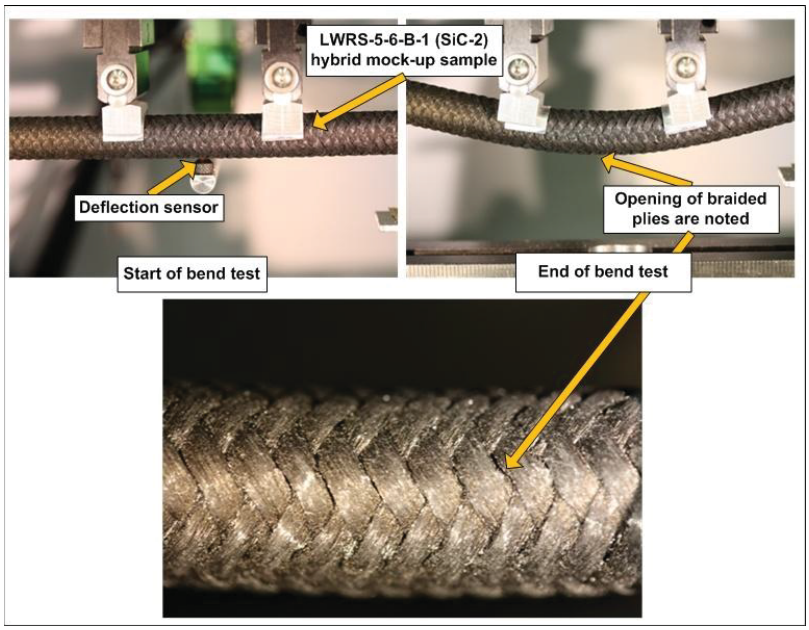

Figure 6. Bend test results of the 7 cycles, 1 ply LWRS-5-6-B-1mock-up sample (SiC-2) at start and end of bend test, showing the opening of the braided plies.

1.5 Quality Requirements

Quality requirements for all test samples are provided in the LWRS Quality Assurance Program Document (QADP) [16]. As some tests were first of the kind and no prior test methods were available, characterization plans and test plans for LWRS experiments will be placed under configuration control in the INL Engineering Document Management System (EDMS) in accordance with LWP-1201 upon updating and approval to allow this work to become a standard test method [17].

The characterization tests and work described in this report are at quality level 3. Work directions were given during a weekly briefing meeting, as well as ad hoc meetings as necessary. Specific pre-job briefings were given in accordance with LWP-9201 [18] prior to the initiation of this work and are recorded in the laboratory notebooks in accordance with MCP-2875 [19]. The bent mock-up samples were received from the LWRS storage cabinet located in INL IRC lab C17 accompanied by the "Activity Sheet". The samples were registered in the lab C17a register and stored in the locked storage cabinet until use. All samples are well numbered and labeled at all times. Characterization routing cards were compiled by the characterization principal investigator (PI) which accompanied the samples to the various characterization activities. (At the moment this is handwritten to determine the usefulness of it, but in future for the actual prototypes it can be recorded in an official document: See Appendix A for a typical example). Results, sketches and notes are recorded in dedicated LWRS characterization laboratory note books. Specific characterization results are also recorded in the specific qualified researcher's notebook. A list of the relevant notebooks is shown in Appendix B. The interpretation and conclusions of all characterization data are reported in technical reports. The EBSD measurements were performed by a qualified researcher.

2. MATERIALS AND METHODS

2.1 Materials

One sample set, comprising of the three bend test samples, was initially investigated as part of this brief study. The three bend test samples included cross section samples from the maximum point of deflection from the 1 ply SiC-CMC hybrid mock-up tube, the 2 ply hybrid SiC-CMC mock-up tube and the standard Zr-4 mock-up tube. Figure 7 provides a schematic of the point from which the samples were obtained. Note that the hybrid mock-up tube samples correspond to the underlying Zr-4 tube and to not include the SiC-CMC overbraid. The first sample set described in detail in a previous report [2]. In this study the original sample numbers were used, namely SiC-1, SiC-2 and SiC-6 for the cross sectioned mounted samples respectively. Various EBSD analyses were completed and are differentiated with a numerical suffix. Qualitative scanning electron microscopy energy dispersive spectroscopy (SEM-EDS) chemical analysis was performed to confirm that the tubes were not Zircodyne, as previous experiments used Zircodyne rather than Zr-4. EDS analyses on the EBSD samples confirmed that these tubes did not contain Nb or Hf percentages typically observed in Zircodyne; therefore, they were most probably Zr-4.

During the investigative process it was decided to include another baseline sample set for comparative purposes, which comprised of a sample prior to bend test and a Zr-4 tube sample annealed at 300ºC for 100 hours. These samples were numbered SiC-5-1 and SiC-5-4, respectively, as it originated from the raw material from the SiC-5 sample described in [2]. More reasoning on the motivation for this addition are described in Section 3.2.1.

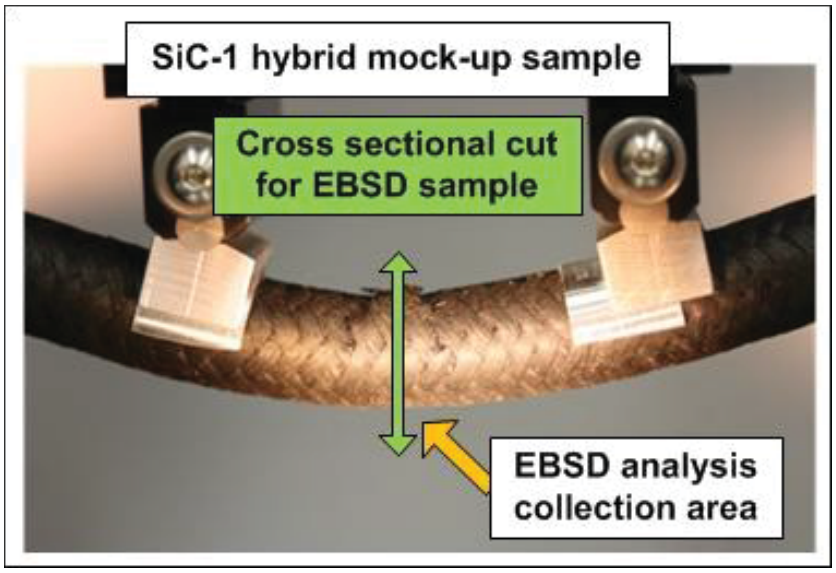

Figure 7. Position of cross-sectional sample taken at point of maximum deflection.

2.2 Characterization Methods

2.2.1 Electron Back Scattered Diffraction (EBSD)

A very short description of the EBSD technique are provided here as introduction to the new reader. A summary paper by Wilkinson and Britton [20] is recommended for further reading on this technique. EBSD is a practical characterization technique to obtain crystallographic information like crystal type, orientation, grain boundary characteristics, grain size distribution and texture. These measurements are obtained from small areas using a scanning electron microscope (SEM). The ability of this technique to perform scanning over a wide range of step sizes makes it possible to investigate the microstructure to nano levels when needed [10].

The EBSD analysis were performed using a FEI Quanta FEG650 SEM using an EDAX TSL Hikari electron backscattered detector with the OMNIA software package version 5.31 for data collection and analysis. The samples were tilted at 70° within the chamber with fine calibration of the detector geometry using the crystal structure for the hexagonal (alpha) Zr phase expected to be present. The confidence index (CI) of the EBSD pattern is calculated during automated indexing of the diffraction pattern. For a given diffraction pattern several possible orientations may be found which satisfy the diffraction bands detected by the image analysis routines. The confidence index ranges from 0 to 1. The confidence index can be a bit misleading and a low CI value does not necessarily mean the EBSD data is not valuable. Typically CI of 0.1 and 0.4 represent a statistical confidence of 95% and 99% respectively [21]. This will be further discussed in Sections 3.2.3 and 3.2.4.

2.2.2 Three-Dimensional Tomography

Three-dimensional tomography was not available at INL during the initial stages of this work. Hence, 3D tomography was only introduced for radiographic examination after the samples were exposed to bend testing. Although the full radiographic examination included for imaging of the gaps found between the SiC-CMC sleeve and the Zr-4 cladding tube, for this study only the images of the Zr-4 tube part was examined.

The 3D Computed Tomography X-ray imaging system at the INL Research Center was designed by North Star Imaging of Rogers, MN. Possibly the most important components of the system are the extremely powerful graphical processing unit housed in the image reconstruction computer and the proprietary image processing software. Additional system components consist of a Hamamatsu 130kVp microfocus x-ray unit capable of producing approximately 10 μm resolution images, a Varian PaxScan flat panel digital x-ray detector, and a rotational stage. (See Appendix C for more detail on equipment capability).

2.2.3 Qualitative Chemical analysis (SEM-EDS)

Qualitative chemical analysis was completed on the three cross sectioned Zr tubes of SiC-1, SiC-2 and SiC-6 to determine only if Hf and Nb were present, which would indicate possible contamination or misidentification of raw material samples. Chemical analysis was executed using a Quanta 650 FEG SEM with the EDAX Triton package. The calibration was performed by the service engineer with a SIRA S170 Certified Test Specimen.

3. RESULTS AND DISCUSSION

3.1 Comparative 3D X-ray Tomography of Mock-up Hybrid Samples after bend test

The maximum deformation of 21% was measured for the SiC-1 Zr-4 tube, with only up to 2% deformation for the SiC-2 tube. Comparatively, the SiC-1 sleeve experiences much higher deformation if compared with those of SiC-2. Figures 8 to 10 show the x-ray tomography images of the Zr-4 tube of the SiC-1, SiC-2 and SiC-6 SiC-CMC-Zr-4 hybrid cladding tubes, respectively, with the measured deformation shown in Table 1. Comparatively, from these images and basic deformation calculations, it is noted that deformation of the Zr-4 tube in the case of the SiC-2 hybrid tube was more restricted by the 1-ply SiC-CMC sleeves. From the results previously reported in [2], cracks were observed in the SiC-CMC sleeve of the SiC-1 sample, but the SiC-CMC from sample SiC-2 did not crack, it only moved. This observation explains the higher constraints (lower deformation) observed for the SiC-2 sample. As reported in a previous report [2], the bend test on the bare Zr-4 tube (SiC-6) showed a shortfall in the initial test, as a maximum deflection value of 10% prohibited the test to continue to a maximum load condition for Zr-4. Therefore the level of deformation observed in Figure 10, is not directly comparable with the results obtained from the bend tests performed on the hybrid mock-up samples.

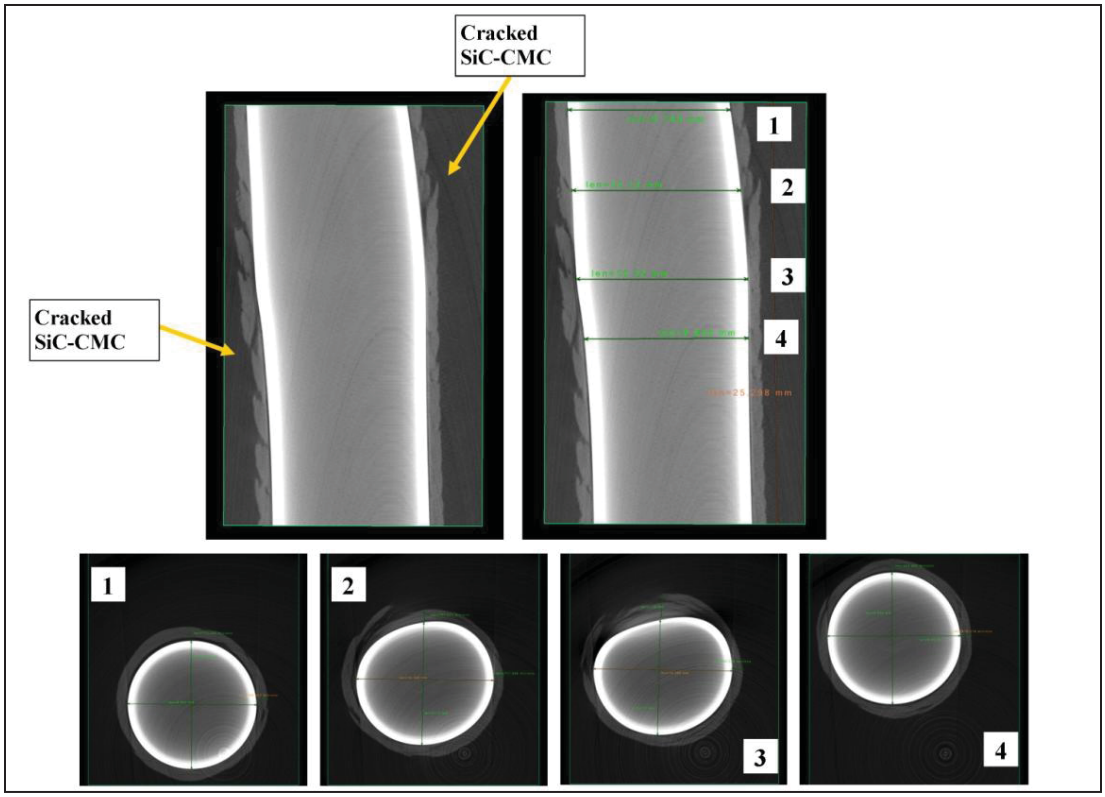

Figure 8. X-ray micrographs of sample SiC-1showing deformation of 0.4; 10.7; 21 and 0.5% at the positions identified as 1, 2, 3 and 4 respectively.

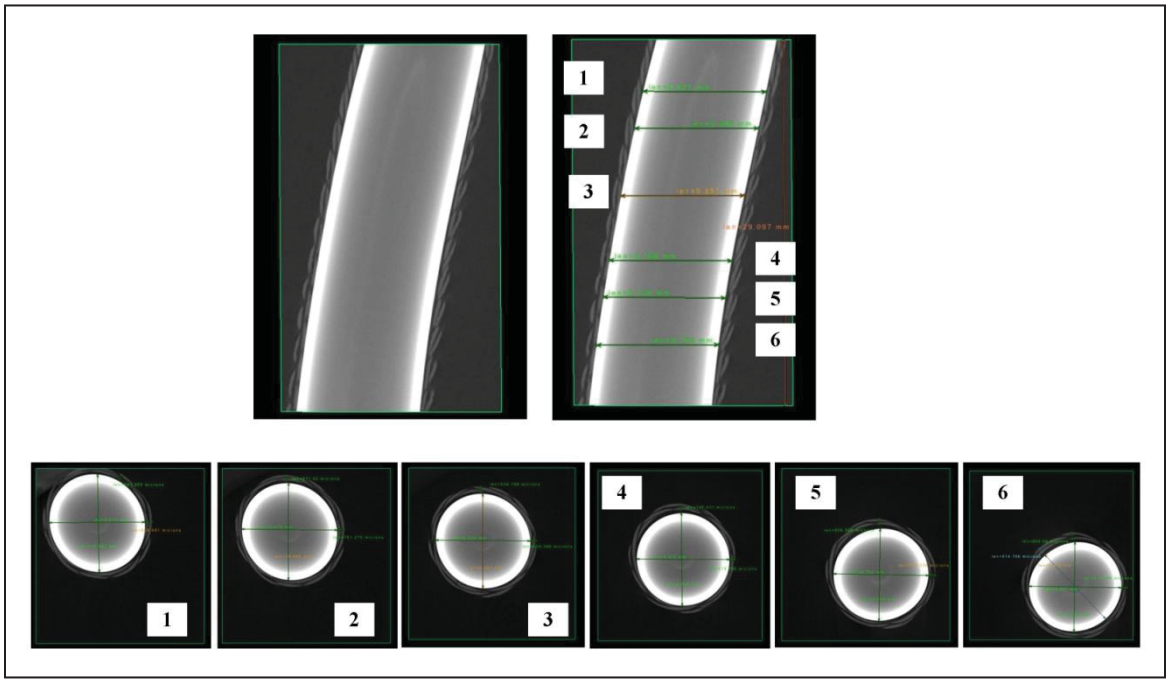

Figure 9. X-ray micrographs of sample SiC-2showing deformation of 2; 1.5; 0.4; 0.6; 1.7 and 1.9% at the positions identified as 1, 2, 3, 4, 5 and 6 respectively.

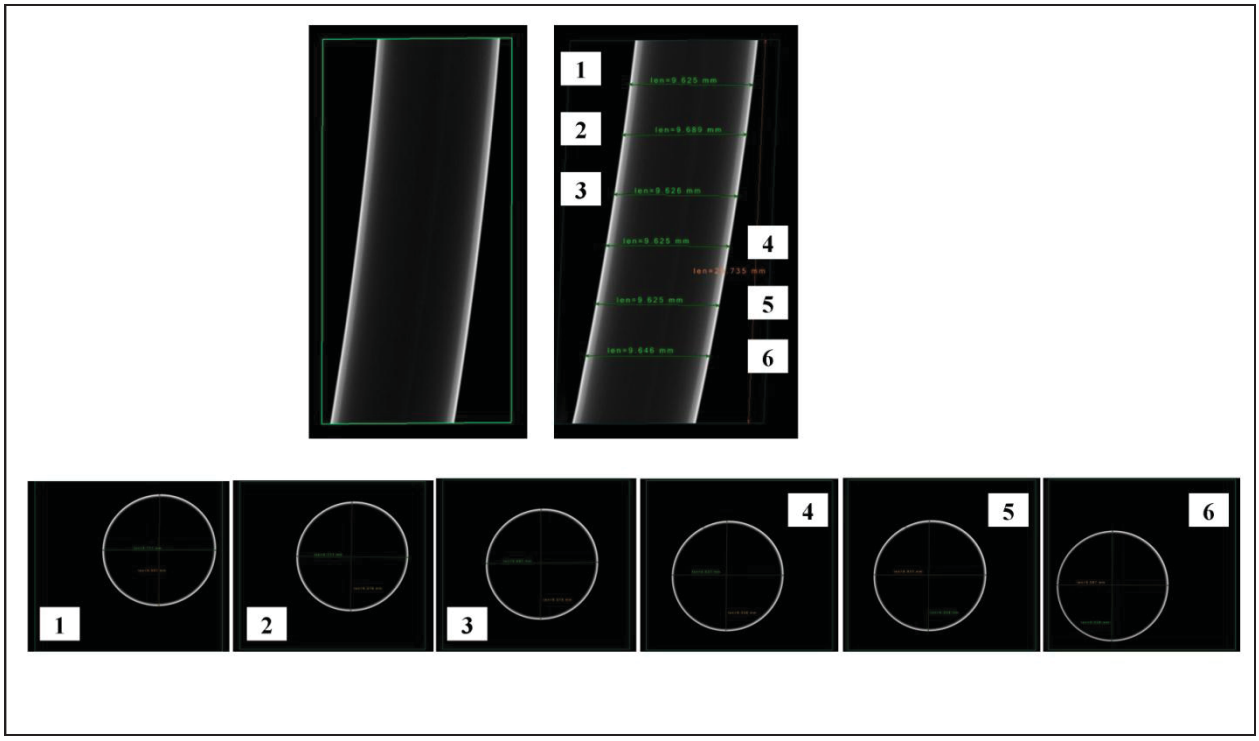

Figure 10. X-ray micrographs of sample SiC-6 showing deformation of 1.5; 1.5; 1.1; 1.1; 0.8 and 0.6% at the positions identified as 1, 2, 3, 4, 5 and 6 respectively.

Table 1. Summarized deformation values based on basic outer diameter change calculations at selected positions at point of maximum deflection.

Sample number	Measurement (mm)	1	2	3	4	5	6
SiC-1	Outer diameter 1	9.566	9.13	8.59	9.844	N/A	N/A
	Outer diameter 2	9.602	10.109	10.398	9.89	N/A	N/A
	% Deformation	-0.38	-10.72	-21.05	-0.47	N/A	N/A
SiC-2	Outer diameter 1	9.792	9.644	9.855	9.897	10.045	10.067
	Outer diameter 2	9.601	9.792	9.812	9.834	9.876	9.876
	% Deformation	1.95	-1.53	0.44	0.64	1.68	1.90
SiC-6	Outer diameter 1	9.591	9.578	9.578	9.578	9.558	9.528
	Outer diameter 2	9.737	9.717	9.687	9.687	9.637	9.587
	% Deformation	-1.52	-1.45	-1.14	-1.14	-0.83	-0.62

Tomography was proven to be a useful tool in identifying open porosity during pre-test characterization. Additionally the benefit of tomography as an indirect tool for establishing simulation parameters such as deformation and SiC-CMC sleeve – Zr-4 cladding tube gap was identified as shown in Figures 11 and 12. These measurements are considered valuable for the validation of the finite element analysis on deformation properties. These short comparative measurements, however, showed the possibility to compare different cladding tube designs for immediate impact on the deformation and clad-tube gap size which could be used for temperature transfer studies. Further incorporation of the tomographic measurements and deformation needs to be explored with the computational simulations group to identify the exact conditions and areas of measurements needed.

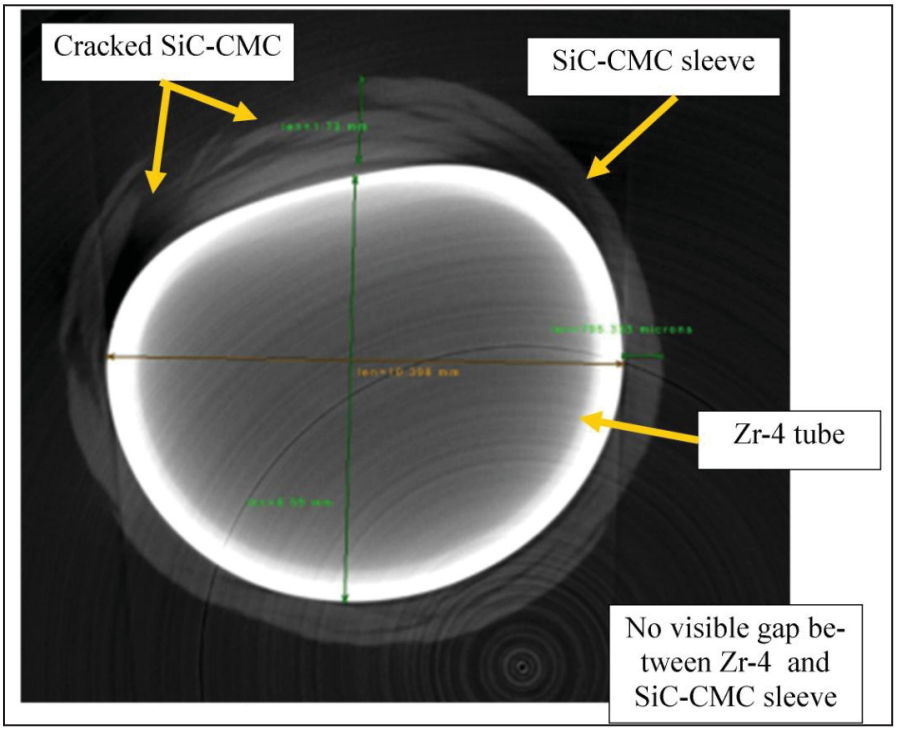

Figure 11. X-ray tomography micrograph of SiC-1showing the cracked fibers at position of maximum tensile stress. This image also shows that there is no gap visible between the SiC-CMC sleeve and the Zr-4 cladding tube. The effect of the distortion (deformation) due to the bend test on the gap is clearly visible in this image.

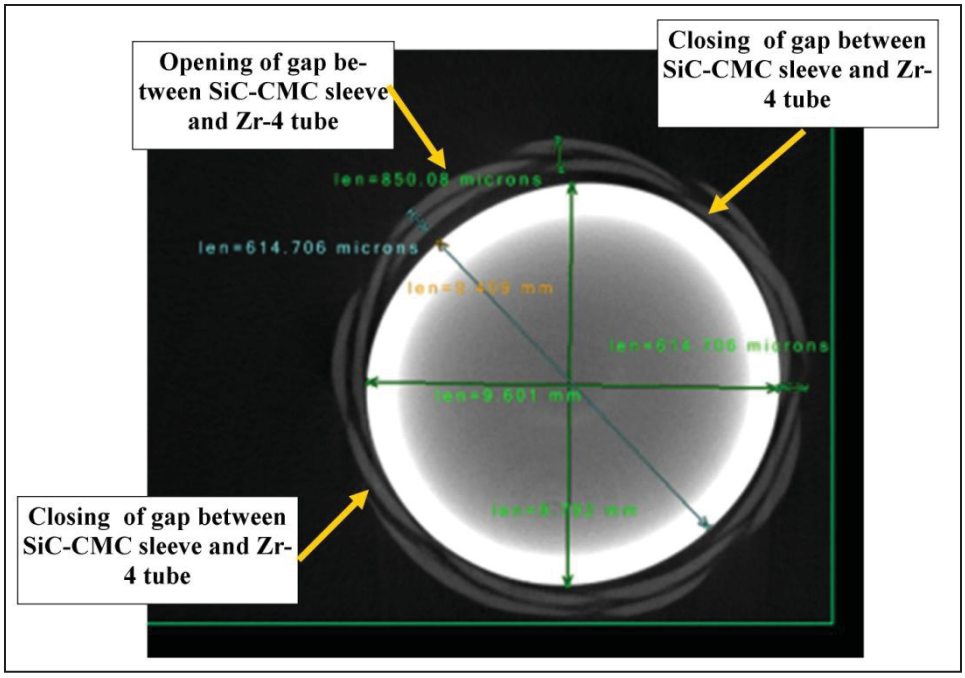

Figure 12. X-ray tomography micrograph of SiC-2 showing the bending of the inner Zr-4 tube and the subsequent closing of gap between the SiC-CMC sleeve and the Zr-4 tube.

3.2 EBSD Examination of Zircaloy Tubes after Bend Test

3.2.1 Sample preparation techniques for EBSD measurements

The sample preparation for EBSD measurements is one of most critical and most difficult steps and highly material dependent. Zirconium-based materials are soft and ductile hexagonal close-packed metals that can deform by mechanical twinning if handled aggressively in sectioning and grinding. Additionally, the grinding and polishing rates are very low and it is very difficult to remove all surface scratches and secondary deformation [22]. For EBSD measurements, relief control is of utmost importance. Because the Zr-4 samples were already deformed due to the bending tests performed earlier, it was expected to be a polishing challenge.

Sample preparation techniques are rarely detailed in journal publications, but most researchers agreed that various iterative steps and approaches were used before a specific successful method was found for the specific samples investigated. Various researchers reported that an iterative polishing-chemical etching technique was used to achieve an artifact-free and low surface roughness surface [12 and 23]. The etchant was in all cases shown as a HF, HNO_3 and H_2O mixture at room temperature with a final polishing step with a colloidal silica/H_2O_2 solution. Some researchers also described the electro-polish to obtain a smooth surface for EBSD measurements [3 and 5].

The sample preparation evolution for this work is briefly described here. As a baseline for this work, EBSD mount preparation techniques used previously for samples LWRS-1-6-A-1 and LWRS-10-482 [2] were considered. For the EBSD mounted cross sectioned samples, the SiC-CMC sleeves remained attachedto the Zr-4 tube, as the aim was also to begin to collect EBSD patterns from both the SiC-CMC and Zr-4. The EBSD technique development for the SiC-CMC sleeves was not completed in the initial work, and the SiC-CMC particulates were detrimental to the polishing of the Zr-4. These challenges led to mounting of only the Zr-4 tubes for this study. The one positive effect that the SiC-CMC sleeve had on

the original sample preparation was that the rounded edge effect on the Zr-4 polished cross section was minimized. To counteract the rounding effect in preparing the bare Zr-4 tubes, the cross sectioned bend samples were potted using the phenol hot mount, as it provides more structure and the rounding that occurs during polishing is generally not significant. However, lengthy sample polishing on these mounts still yielded a rounded edge effect typically found due to the difference in hardness between the mount material and the material to be analyzed.

At this point, consideration was given to the difficulty in obtaining images after the lengthy polishing techniques previously found to be successful for other Zr-4 EBSD samples. The following uncertainties were considered as potential causes:

1. Is this tube material actually Zr-4 material? What were the processing parameters used during tube fabrication?
2. Was deformation too high to obtain EBSD images?
3. Were non-optimum polishing techniques and EBSD set up parameters used?

Uncertainty 1 was raised due to previous quality problems related to mixed Zirconium based materials as well as the fact that complete tube fabrication details were unknown. . Fabrication history was requested from the supplier and only brief statements were received indicating that it most probably was only stress relieved but not recrystallized. Qualitative chemical EDS analysis showed that this material was not a Hf based material and therefore most probably Zr-4. Uncertainty 2 was not considered to be the major source of difficulty, as a literature survey provided examples of EBSD on deformed Zr-4 structures [10]. Although uncertainty 3 was considered to be the main reason for not achieving EBSD measurements initially, the traceability of the tube fabrication history was still a nagging issue and it was considered that the Zr-4 tubes could have been received without any stress relieving heat treatment. It was therefore decided to prepare a baseline sample set inclusive of an as-received Zr-4 tube, and then a range of Zr-4 tubes heat treated to known conditions. These included a stress relieved sample and annealed to 300^{o}C for 100 hours for a simulated effect of initial exposure in a LWR.

Initial mounting and polishing on these heat treated samples in Al_2O_3 mixed with the epoxy resolved the rounding effect, but charging during imaging posed a large problem, even when the sample was C-coated. In attempt to solve this, tungsten particles were embedded into the epoxy. It was believed that the tungsten particles were not large enough to be retained in the epoxy and created a substandard finish on the sample. A successful preparation technique was found by using a graphitic conductive mount material, KonductoMet, which resolved the charging problems. The edge effects and smoothing of the surface was resolved using an iterative process of polishing and chemical attack as shown in Table 2. Although EBSD images could be obtained with this technique, further improvements were made and image quality was improved with the techniques described in Table 2. Based on the success on samples SiC-5-4 and SiC-5-1, the second half of the three bend test samples were mounted in the graphite material and prepared using the method applied to sample SiC-5-1. Irrespective of the success obtained in this SiC-5-1 sample, still further preparation modifications was necessary. Generally an additional vibratory polishing step from 12 to 13 hours was necessary to obtain average quality EBSD images.

All the sample mounts are shown in Figure 13, with a summarized preparatory description in Table 2. The sample evolution timeline is provided in the table; a more detailed timeline history is provided in Appendix D. The SEM micrographs in Figure 14 show the polished microstructures of the point of maximum bend deflection of the SiC-1, SiC-2 and SiC-6 Zr-4 tubes, respectively (The top of these images represents the maximum deflection point and EBSD measurements were completed in these areas).

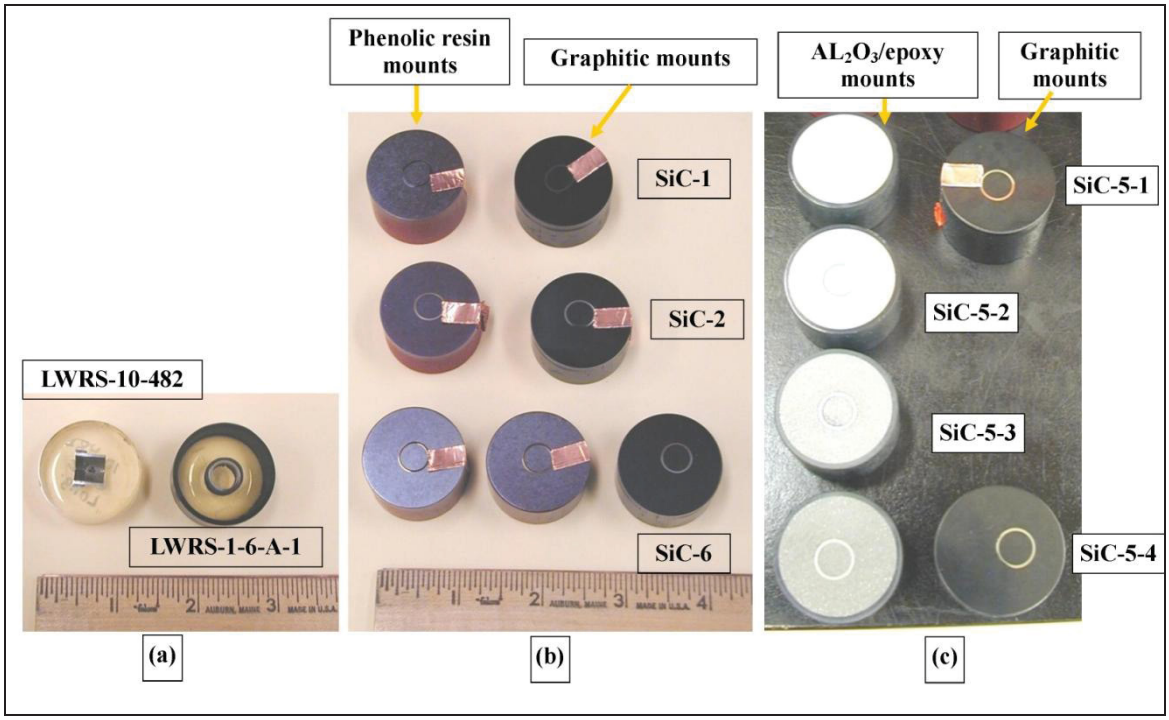

Figure 13. Micrographs showing the various mount materials used for this work showing (a) LWRS-10-482 and LWRS-1-6-A-1 Zircodyne epoxy mounts; (b) phenolic resin and graphitic mounts of SiC-1, SiC-2 and SiC-6 Zr-4 cross-sections and (c) Al_2O_3/epoxy and graphitic mounts of SiC-5-1 to SiC-5-4 Zr-4 cross-sections.

Table 2. Summarized EBSD sample preparation history and some literature baseline summary.

Material	Mount	Preparation Technique	Lessons Learned	Reference
Zr-4 (Optical)	Not reported	1. Polish 0.05 µm colloidal silica H_2O_2 solution 2. Etching 5% HF, 45% HUO_3 and 50% H_2O 3. Final polish colloidal silica H_2O_2 solution	Not reported	[24]
Zr-4 (EBSD)	Epoxy	1. Polish to 400 grit 2. Chemical polishing 45 H_2O:45 HNO_3:10 HF 3. 10 parts 0.05 µm colloidal silica, 1 part H_2O_2 to minimize relief	Not reported	[12]
Zircodyne 702 LWRS-10-482	Epoxy Longitudinal Section	1. Polish (no detail available) 2. 0.3 µm alumina slurry 3. Electropolish 4. Etch HNO_3-HF mixture	Recommended sandwich mount Rounding and bowing experienced	[3]
Zr-Hf based alloy LWRS-1-6-A-1-1 (γ irradiated 50ºC, 167 h)	Epoxy Cross section	1. Polish (no detail available) 2. 0.3 µm alumina slurry 3. Vibratory polish with 0.05 µm colloidal silica (Appendix E)	SiC-CMC sleeve act as retainer, help with movement SiC-CMC caused debris and scratches on Zr surface	[3]
Zr-4 SiC-1	Phenolic resin (red)	1. Polish (not recorded by microscopist)	Rounding experienced	This work.

Material	Mount	Preparation Technique	Lessons Learned	Reference
SiC-6-1 Sic-6-2	Cross section	2. 4 h vibratory polish with 0.05 μm colloidal silica and H_2O_2 chemical attack 3. Vibratory polish with 0.05 μm colloidal silica		
Zr-4 SiC-5-1, SiC-5-4	Alumina and epoxy Cross section	Not recorded by microscopist	Charging no collection	This work.
Zr-4 SiC-5-4-1, SiC-5-4-2	Graphitic Cross section	1. 600 grit ground 2. 9 μm polycrystalline diamond paste 3. 3 μm polycrystalline diamond paste 4. 0.05 μm colloidal silica, chemical attack H_2O_2 5. Additional 20 h vibratory polish with 0.05 μm colloidal silica	5-4-1:Collect data set, low quality 5-4-2: Full data set: average quality	This work.
Zr-4 SiC-5-1 SiC-5-1-1 SiC-5-1-2	Graphitic Cross section	1. 600 grit ground 2. 9 μm polycrystalline diamond 3. 3 μm polycrystalline diamond 4. 0.05 μm colloidal silica, chemical attack H_2O_2 5. 4 h vibratory polish with 0.05 μm colloidal silica 6. 5 h vibratory polish, 0.05 μm colloidal silica 7. 8 h vibratory polish< 0.05 μm colloidal silica 8. (Appendix F)	5-1: Partial data set 5-1-1:Partial data set 5-1-2: Full data set low quality	This work
Zr-4 SiC-6-10 SiC-6-11 SiC-6-12 SiC-1-10 SiC-2-10	Graphitic Cross section	1. 320 grit Sic 2. 9 μm Meta DiSupreme diamond suspension 3. 3 μm Meta DiSupreme diamond suspension 4. ~0.05 μm MasterMet colloidal silica plus attack polish (2 parts 30% H_2O_2, 8 parts MasterMet colloidal silica) 5. 4-13 h vibratory polish, 0.05 μm colloidal silica 6. (Appendix F)	Minimum 12 h required to provide average EBSD results.	This work

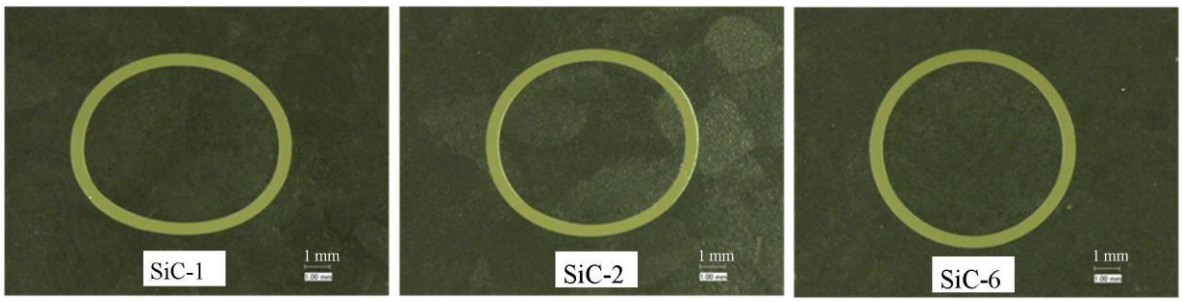

Figure 14. SEM Micrographs showing the polished microstructures of the point of maximum bend deflection of the SiC-1, SiC-2 and SiC-6 Zr-4 tubes respectively (The top of these images represents the maximum deflection point and EBSD measurements were completed in this areas).

3.2.2 Optical Microscopy

The microstructures of the SiC-1 to SiC-6 cross sectioned samples were examined for potential visible deformation on the grains as shown in Figure 15. Due to the small grains, optical microscopy did not provide visual information on grain deformation as shown in Figure 15.

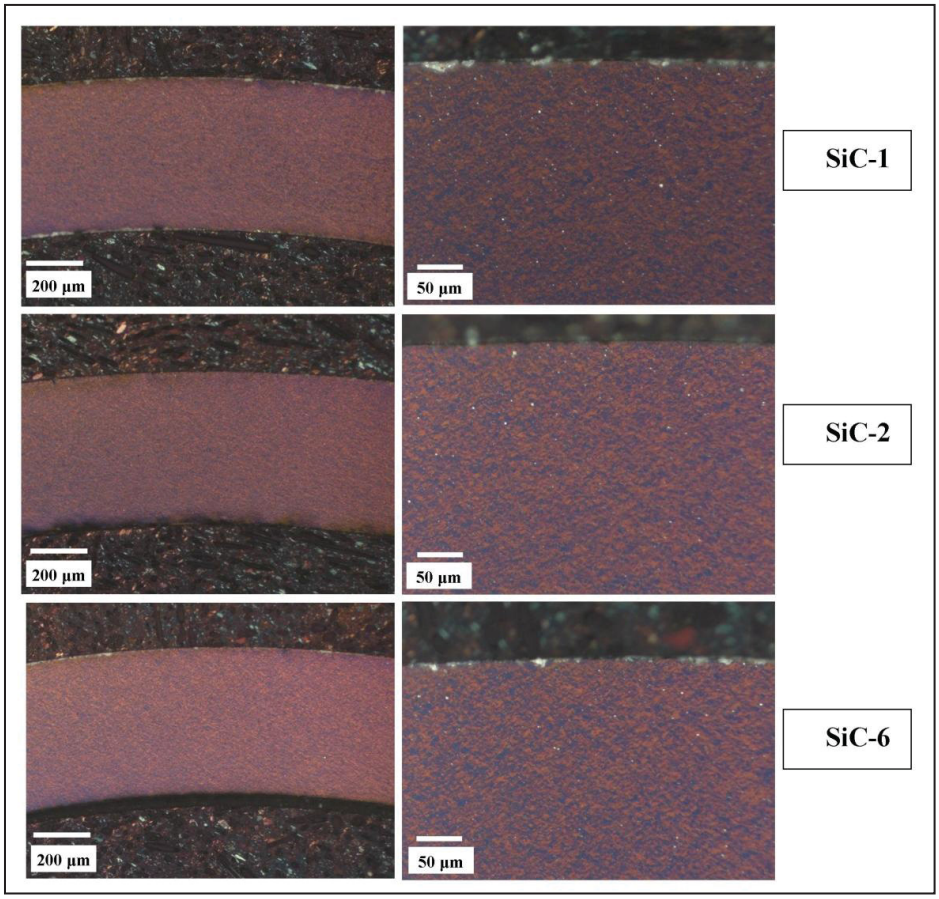

Figure 15. Micrographs showing the etched microstructures of the top part of maximum bend deflection of the SiC-1, SiC-2 and SiC-6 Zr-4 tubes respectively. Due to the small grained structures, no visual effects or comparative differences were observed.

3.2.3 EBSD image evolution and measurement parameter history

As described in the previous section, a number of preparation steps were performed to obtain optimum EBSD images and measurements. In all cases, the EBSD data collection was performed using a 20 kV accelerating voltage and a 30 μm aperture. A summarized EBSD parameter history is shown in Table 3 with examples of the image evolution in the subsequent sub-sections. The EBSD parameters in Table 3 are listed in time sequence to demonstrate the changes in the parameters more clearly. The best average CI obtained for the bend test samples was 0.5, comparatively lower than those for the annealed sample and as-received sample of 0.80 and 0.69, respectively. These maximum average CI values were achieved with optimized preparation techniques and EBSD parameters. The improvement noted for the heat treated sample (SiC-5-4) was 48% and 20% for the sample (SiC-5-1) in the as received condition and the evolution of the EBSD microstructures are shown in Figures 16 and 17. The improvement in EBSD image quality showed an improvement of 76 % and 85 %, respectively, for the SiC-1 and SiC-6 bend test samples as shown in Figures 18 and 19. Based on the lower average CI achieved on the measurement points of the bend samples and previous research from Krisna, *et al*. [10], the cleaning operation was performed with a CI of 0.1 which corresponds to an approximate 95% statistical confidence level. It should further be noted that Krisna, *et al*. [10] used a CI of only 0.03 for the research on Zircaloy at various stages of the fabrication process. Most researchers of the studied publications gave no indication of the CI used for their EBSD data.

Table 3. Summarized EBSD data collection and measurement parameter history.

Sample No.	Step size (μm)	Spot size (μm)	Collection area (μm^2)	Working distance (μm)	Average CI	Cleaning CI
SiC-1	0.1	6	25x70	14	0.12	0.4
SiC-6-1	0.2	6	50x80	14	0.27	0.4
SiC-6-2	0.2	6	50x80	13	0.06	0.4
SiC-5-4-1	0.1	5	20x30	14	0.42	0.4
SiC-5-4-2	0.1	4	20x30	14	0.80	0.4
SiC-5-1-2	0.1	4	20x30	15	0.55	0.4
SiC-5-1-3	0.1	4	20x30	17	0.69	0.4
SiC-6-10	0.1	4	20x30	11	0.4	0.1
SiC-1-10	0.1	4	20x30	12	0.45	0.1
SiC-1-11	0.1	4	20x30	12	0.5	0.1
SiC-2-10	0.1	4	20x30	11	0.4	0.1

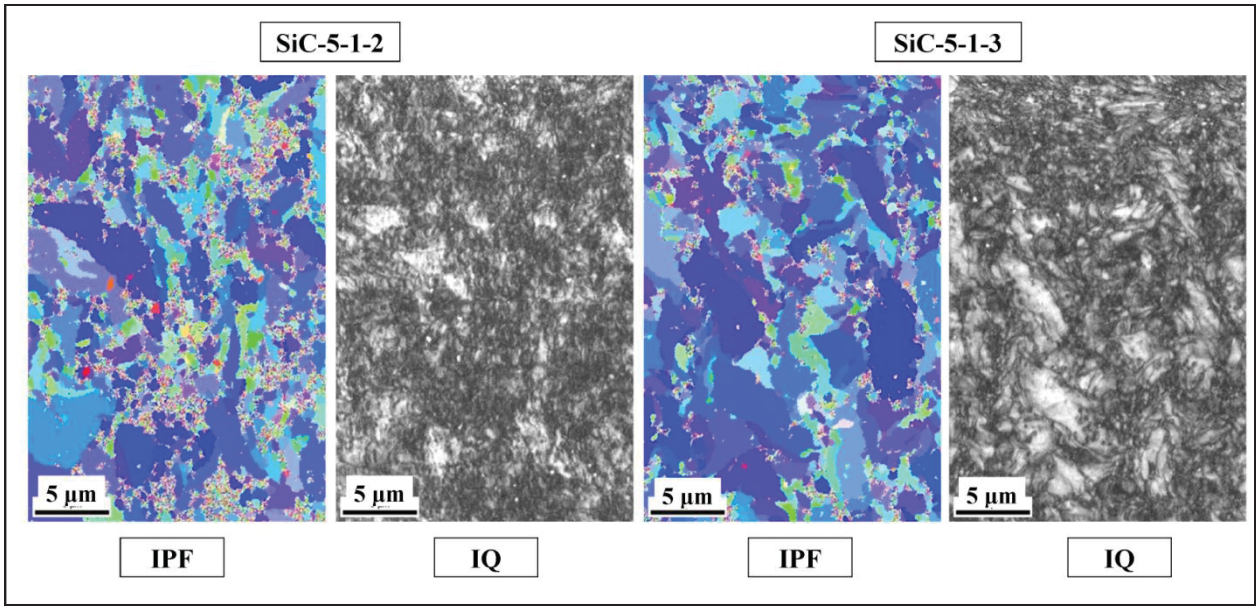

Figure 16. Micrographs showing the evolution of the EBSD measurements; Inverse pole figure (IPF) and Image quality (IQ); of the sample (SiC-5-1) in the as received condition. The average CI improved with 20% from SiC-5-1-2 and SiC-5-1-3.

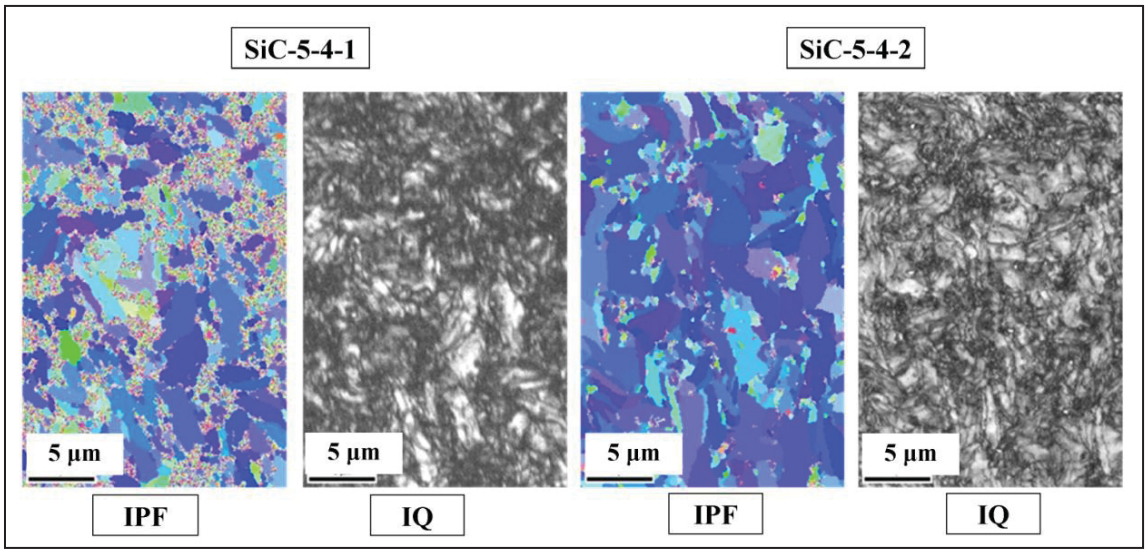

Figure 17. Micrographs showing the evolution of the EBSD measurements; IPF and IQ; of the heat treated sample (SiC-5-4) and the improvement on average CI was 48%.

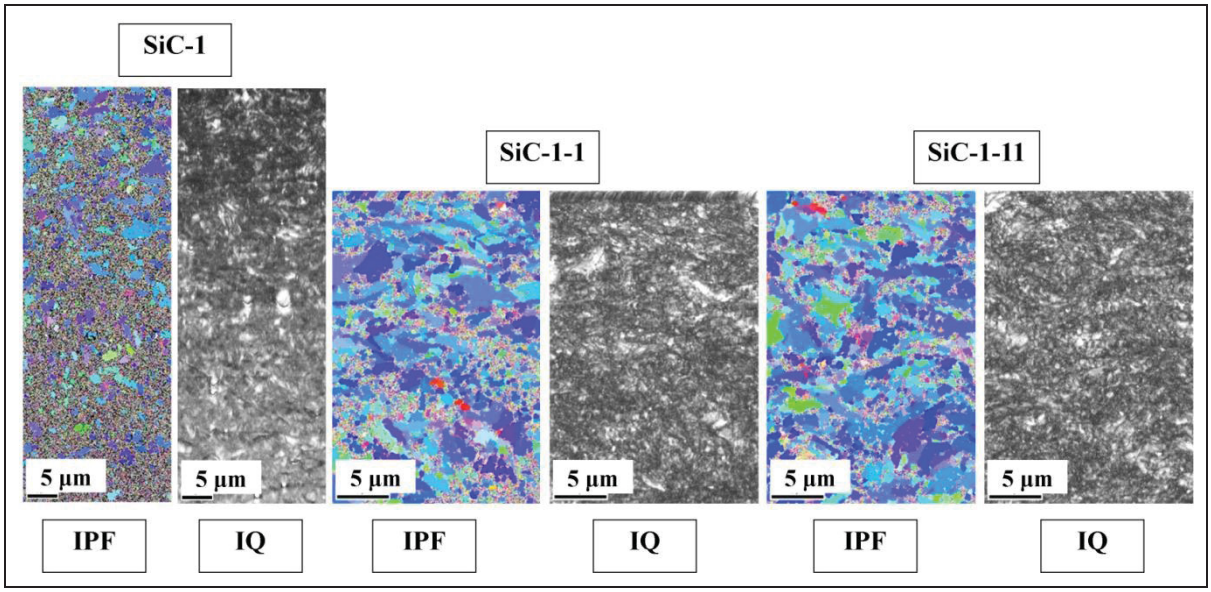

Figure 18. Micrographs showing the evolution of the EBSD measurements; IPF and IQ; of the SiC-1 sample after bend at the point of maximum deflection. The average CI improved with 76% from SiC-1and SiC-1-11.

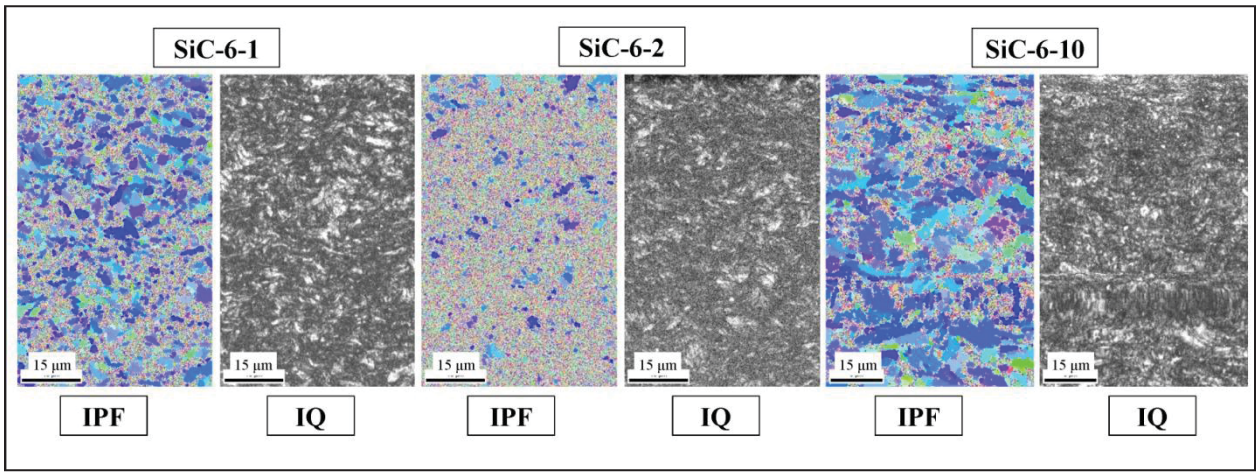

Figure 19. Micrographs showing the evolution of the EBSD measurements; IPF and IQ; of the SiC-6 sample after bend at the point of maximum deflection. The average CI improved with 85% from SiC-6-2 and SiC-6-10.

3.2.4 Comparative EBSD measurements

3.2.4.1 Grain structure and size (Inverse pole figures (IPF), Image quality (IQ))

The EBSD measurements were performed near the outer edge of the samples to capture information at the area of maximum stress and deformation, as shown in Figure 20. The direction numbering used in the pole figures (TD and RD), are also shown to show the relationship to the analysis area. Care needs to

be taken as these directions do not correspond to the fabrication rolling direction. These samples are cross sectional to the fabrication longitudinal direction. The color coded map for the inverse pole figures is shown in Figure 21.

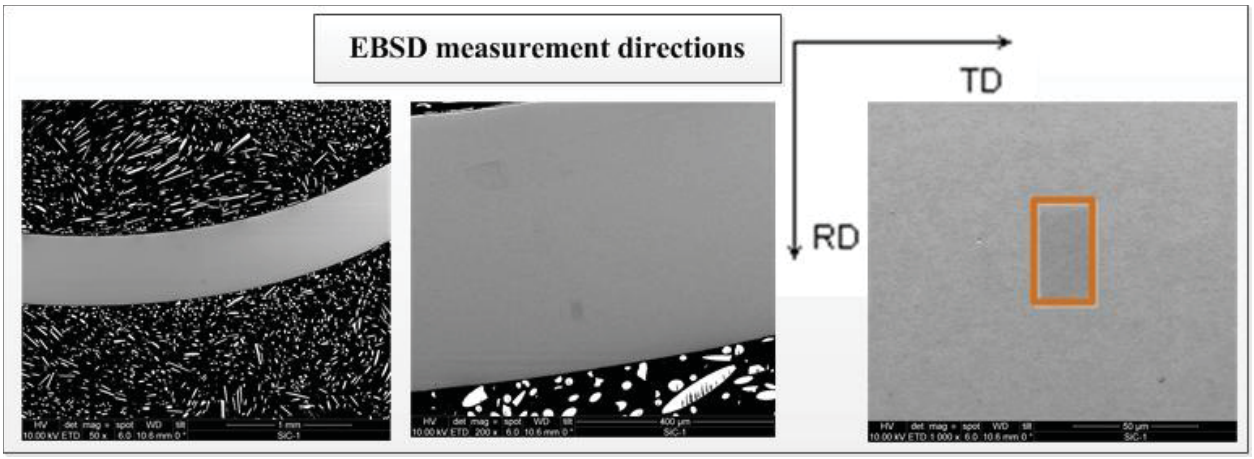

Figure 20. Micrographs showing the position of EBSD measurements near the outer edge of the samples to capture information at the area of maximum stress and deformation. The direction numbering used in the pole figures (TD and RD), are also shown to show the relationship to the analysis area. Care needs to be taken as these directions are not corresponding to the fabrication rolling direction. These samples are cross sectional to the fabrication longitudinal direction. (Micrographs used as an example are from SiC-1)

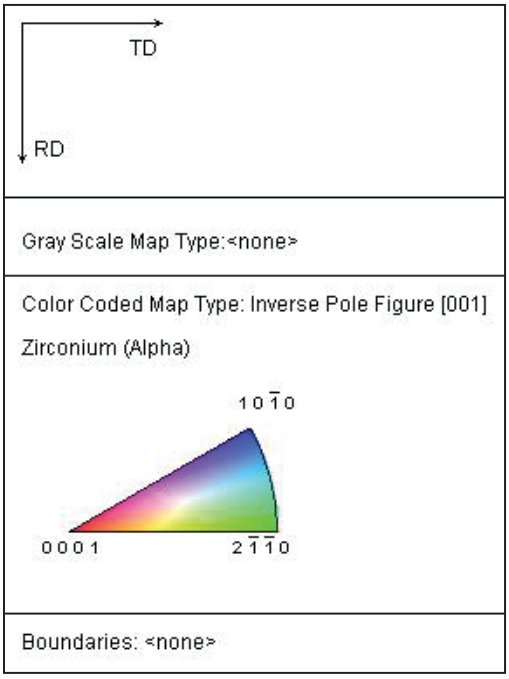

Figure 21. Pole figure color coded map for Zirconium (Alpha)

From the IPF and combined IPF & IQ graphs shown in Figure 22, the effect of the bend test can be clearly seen. The grain structures seen for SiC-5-1 and SiC-5-4 samples are a mixed equiaxed and elongated structure in the RD direction with average sizes of 1.93 µm and 2.00 µm, respectively. The elongated grains are aligned parallel to the extrusion fabrication process. Comparatively, the grain structures for the three bend samples are more equiaxed with average sizes of 1.24 µm, 1.1 µm and 1.25 µm for SiC-1, SiC-2 and SiC-6, respectively. Typically, the EBSD sample preparations for smaller grained samples are more challenging, as was also experienced in this case. No conclusion could be made on the comparative grain size distribution and spread as shown in Table 4 (Appendix G detail graphs on grain size distribution). Additionally, no correlation was visible between the average grain size and the deformation level due to bending. A preferred orientation along the 10-10 plane is observed for all the samples, although the orientation in the bend samples suggested a small change towards orientation in the 0001 and 2-1-10 planes due to the deformation caused by the bending of the samples.

Table 4. Summary of grain size measurements.

Sample No.	% Deformation by Bending	Average grain diameter (µ m)	Standard Deviation	Max Grain Size (µm)
SiC-1-11	21	11.2	0.37	3.1
SiC-2-10	2	11.1	0.33	4.1
SiC-6-10	1.5	11.3	0.37	3.5
SiC-5-1-3	0	22.0	0.52	4.9
SiC-5-4-2	0	11.9	0.56	4.1

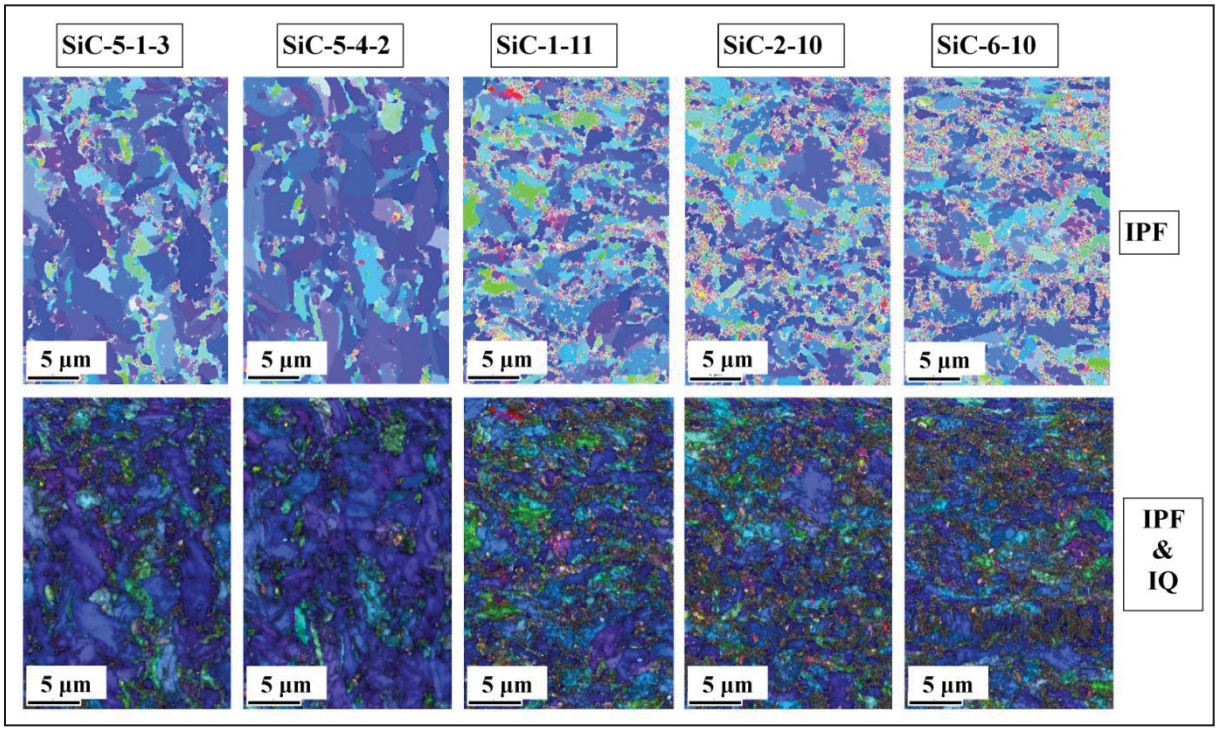

Figure 22. Micrographs showing the comparative inverse pole figures and the combined IPF and IQ figures.

3.2.4.2 Misorientation Angles and Grain Boundary Character Distribution

The average misorientation angles and grain boundary character distribution of the 5 samples were determined and are reported in Table 5. The average misorientation angle provides average misorientation between neighboring measurement points in a grain. Although the average misorientation angle is lower for the bend samples, no conclusion could be reached based on these results. Comparatively, the grain boundary distribution character obtained from the bend samples is different from the annealed and as-received sample. The bent samples exhibit a larger number fraction of angles lower than 15 degrees. From these bent hybrid samples, SiC-1 (two ply hybrid sample) contains a lower fraction of low angle grain boundary characters, and a higher corresponding average misorientation angle of the grains. This is indicative of the higher amount of deformation visually observed from Figure 15. The graphical display of the misorientation angles and grain boundary character distribution are shown in Appendix H and I; respectively.

Table 5. Summarized EBSD data collection and measurement parameter history.

Sample No.	Average misorientation angle (degrees)	Grain boundary character distribution (Number fraction)	
		0.3≥ angle≤ 15	15
SiC-5-1-3	38.4	0.17	0.82
SiC-5-4-2	38.2	0.14	0.85
SiC-1-11	36.5	0.21	0.79
SiC-2-10	33.3	0.27	0.73
SiC-6-10	32.2	0.29	0.71

3.2.4.3 Pole Figures

Comparative pole figures for all samples are presented in Figure 23 showing the texture evolution as a function of bend deformation and the effect that the SiC-CMC sleeve had on the Zr-4 tube texture. The relevant texture keys are available in Figure 24.

Compared to the baseline SiC 5-1-3 sample (Figure 23 (a)), localization and stronger 0001 texture development alongside the RD direction are noticed for the deformed SiC-1-11 and SiC-2-10 samples (Figure 23 (c) and (d)). Interestingly, however, is that it is more prominent for the lower deformed SiC-2-10 sample compared to the higher, 21% deformed SiC-1-11 sample. This is not fully understood yet. No specific alignment towards a specific direction is noted for the SiC-6-10 sample (Figure 23 (e)).

An alignment of grains parallel to the 2-1-10 TD direction is also suggested for the bend samples. Similar to the finding in the 0001 texture, no directional alignment for the 2-1-10 textures was noted for the SiC-6-10 sample (Figure 23 (e)).

No specific comparative changes were noted for the 10-10 textures. Additionally, no significant changes were observed when comparing the pole figures from the annealed baseline with the un-annealed baseline samples ((a) and (b) in Figure 23).

SiC-5-1-3 0% Bend Deformation Baseline	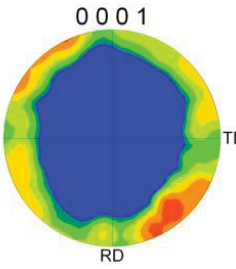 (a)	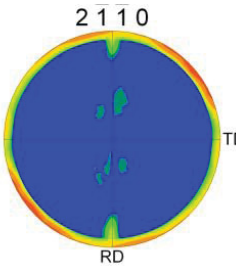 (a)	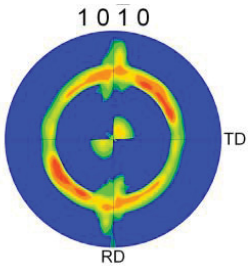 (a)
SiC-5-4-2 0% Bend Deformation Annealed 300ºC, 100 h	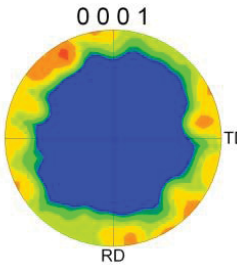 (b)	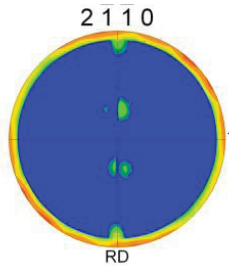 (b)	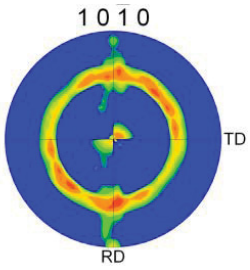 (b)
SiC-1-11 21 % Bend Deformation	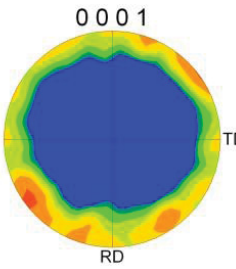 (c)	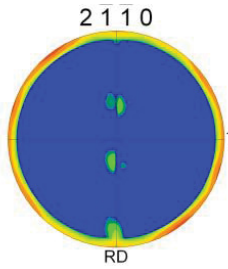 (c)	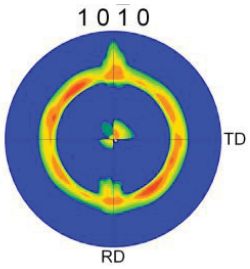 (c)
SiC-2-10 2 % Bend Deformation	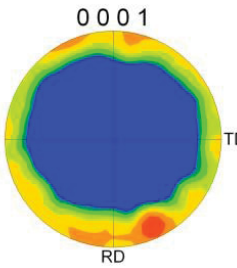 (d)	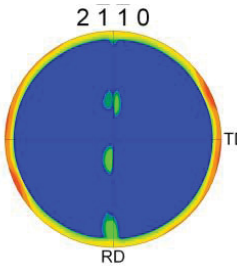 (d)	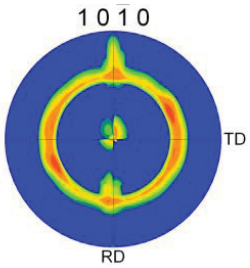 (d)
SiC-6-10 1.5 % Bend Deformation	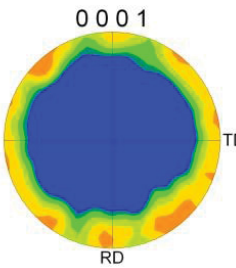 (e)	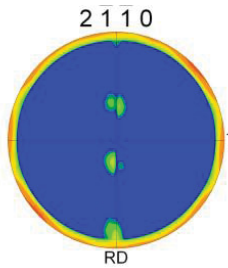 (e)	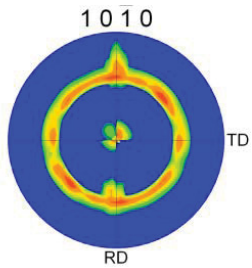 (e)

Figure 23. Comparative pole figures showing texture evolution as a function of bend deformation and the effect of the SiC-CMC sleeve on the Zr-4 tube texture.

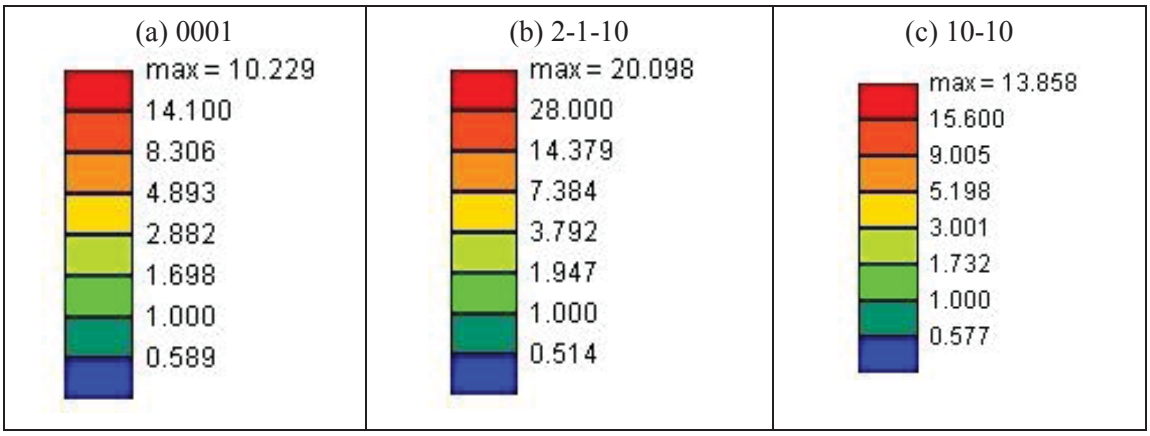

Figure 24. Texture indexing to the pole figures presented in Figure 24.

4. LESSONS LEARNED

This feasibility study provided many lessons learned which may help increase the effectiveness in future work:

1. Initial delays in collecting the EBSD data were identified and are listed as follows:
   - Smoothness of polished surface due to property (hardness, ductility) differences between the mount material and the actual sample material.
   - Obtaining patterns in deformed Zircaloy material is more challenging than for non-deformed tube (most probably with mechanical twinning present), therefore appropriate time needs to be allowed for this activity.
   - Image quality in small grained material is reduced due to mixed diffraction patterns from two adjacent grains.
   - Charging of the surfaces results from poor conductivity.
   - Rapid surface oxidization after sample preparation.
   - Microscopy resource availability.
   - Image quality in strained locations containing many dislocations and twinning is reduced due to mixed diffraction patterns.
2. The legacy of unknown condition and quality of the Zr-4 tubing caused uncertainty and additional work which was not planned. Future studies would be improved through the acquisition of traceable material, or additional time needs to be allowed for verification of these materials in all characterization activities.

5. CONCLUSIONS

5.1.1 3D X-Ray Tomography as Plasticity Measurement Technique after Bend Test

The benefit of tomography as an indirect tool for establishing simulation parameters such as deformation and SiC-CMC sleeve-Zr-4 cladding tube gap was clearly identified in this study. These measurements are considered valuable for the validation of the finite element analysis on deformation properties. An additional and significant benefit of these measurements as a non-destructive examination is that the specific levels and locations of deformation can be identified. This may assist in:

- Identifying the correct area of interest for cross sectioning for the electron microscopic characterization.
- Comparative measurements to evaluate different cladding tube designs for immediate impact on the deformation and clad-tube gap size.

Further incorporation of the potential measurements and deformation needs to be explored with the computational simulations group to identify the exact conditions and areas of measurements needed. For example, linkage of the sleeve-tube gap location and dimensions with heat transfer modeling studies and specific Zr-4 tube texture which may assist in failure mode determination and estimations.

5.1.2 EBSD as Plasticity Measurement Technique after Bend Test

The feasibility and value of EBSD measurements as a deformation indicator has been demonstrated in this study. Comparative images and measurements were obtained suggesting the texture changes due to deformation, as well as demonstrating the impact of different sleeve designs. Although the data obtained in this study cannot be used as a quantitative measure at this time, it provides the basis to show that differences are present and measureable.

This feasibility study additionally provides very valuable information on the sample preparation techniques and EBSD parameters needed for deformed Zircaloy material under these bend conditions. This will decrease preparation time for future similar work if pursued further.

5.1.3 Final Conclusion: Meeting the objectives of this study

The value of this report is measured and summarized against the objectives of these mock-up sample tests as follows:

- Details of the EBSD measurements performed on the various sample sets are provided with preliminary conclusions where applicable.
- Details of the EBSD sample preparation and parameters are provided as a baseline for future INL work.
- Three-dimensional tomography cross sectioned images were generated for the Zr-4 tube at various deflection points and baseline localized deformation measurements were performed.

This work provides a solid baseline for future work as often the sample preparation is proven to be the most crucial part of the research, which was overcome in this study.

6. RECOMMENDATIONS

It is recommended that a more detailed analysis be performed on the current data set to study the finer nuances of structure and texture as affected by deformation. Re-analysis of the current data set may also be beneficial to identify possible twinning and the orientation of twin boundaries as a function of deformation level and SiC-CMC sleeve design. This will provide more detail on the deformation mechanisms and effect of the different layers may have on the deformation mechanisms.

Although localized texture changes were observed, it would be interesting to include bulk texture analysis using XRD techniques. Results could then provide a macroscopic perspective on the deformation mechanism.

With the expansion of the EBSD measurements to include more EBSD measurement locations to have a complete Zr-4 layer thickness data set, will be beneficial for further application of these data set for performance prediction. This will provide information on the transition point between compression and tensile stress areas at the point of maximum deflection.

Also recommended is the ful integration of the 3D tomography and EBSD texture information in locations of significant SiC-CMC sleeve –Zr-4 gaps. The quantification of grain size distribution, grain boundary character and grain orientations may also be further explored for significance towards the heat conductivity profiles of the performance tools. Work by Wilkinson *et al.* [13] indicated that wide –angle EBSD patterns can be analyzed to obtain strain and rotation tensor components with high strain rate sensitivity and high spatial resolution. This technique enables elastic strain tensor measurements at the nano level which will provide value to the interface modeling of new clad systems to nuclear cladding tubes.

The finalization of the EBSD technique for hydrogen embrittlement identification is also strongly recommended. This necessitates the controlled hydrogen gas embrittlement studies with EBSD analyses to set a standard.

As the comparative images and measurements obtained in this feasibility study suggested texture changes due to deformation, this study demonstrated the impact of different sleeve designs. It is therefore strongly recommended to continue with this work, to enable the program to develop a powerful performance measurement tool for downstream selection of cladding designs.

7. REFERENCES

[1] PLN-3971 Project Execution Plan for the Light Water Reactor Sustainability (LWRS) Advanced LWR Nuclear Fuel Development Pathway experiments in the ATR

[2] Van Rooyen, Isabella J., INL/EXT-12-27189; Pre-Irradiation Testing and Analysis to Support the LWRS Hybrid SiC-CMC-Zircaloy-4 Unfueled Rodlet Irradiation

[3] Van Rooyen, Isabella J.; Trowbridge, Tammy T; Lilo Tom; EBSD Applications to Predict Nuclear Fuel Performance, INL/CON-12-26393

[4] Kaschner, G. C.; Bingert, J. F.; Liu, C.; Lovato, M. L.; Maudlin, P. J.; Stout, M. G.; Tomé, C. N.; Mechanical Response of zirconium—II. Experimental and Finite Element Analysis of Bent Beams, Acta mater 49 (2001) 3094-3108

[5] Xu, F.; Lattice Strain and Texture evolution during room temperature deformation in Zircaloy-2; PhD Thesis, Department of Mechanical and Materials Engineering, Queens University, Kingston, Ontorio, Canada, December 2007

[6] Kamaya, M.: Assesment of local deformation using EBSD: Quantification of accuracy of measurement and definition of lacal gradient, Ultramicroscopy 111 (2011) 1189 – 1199.

[7] Cockeram, B. V.; Chan, K. S.; In situ studies and modeling of the deformation and fracture mechanism for wrought Zircaloy-4 and Zircaloy-2 as a function of stress-state, Journal of Nuclear materials 434 (2013) 97-123

[8] Xu, C.; Xu, S.W.; Zheng, M.Y.; Wu, K.; Wang, E. D. Wang; Kamado, S. ; Wang, G. J.; Lv, X.Y.; Microstructures and mechanical properties of high-strength Mg-Gd-Y-Zn-Zr alloy sheets processed by severe hot rolling; Journal of Alloys and Compounds 524 (2012) 46-52

[9] Sahoo, S.K.; Hiwarkar, V.D. Hiwarkar, Majumdar, A.; Samajdar, I.; Pant, P. Dey, G.K. Srivastav, D.; Tiwari, R.; Banerjee, S.; Presence and absence of significant twinning: Effects on cold deformed microstructures of single phase Zircaloy 2, Materials Science and Engineering A 518 (2009) 47-55

[10] Krishna, K. B. Mani; Sahoo, S. K.; Samajdar, I.; Neogy, S.; Tewari, R.; Srivastava, D.; Dey, G. K.; Das, Gaur Hari; Saibaba, N.; Banarjee, S.; Microstructural and textural developments during Zircaloy-4 fuel tube fabrication; Journal of Nuclear Materials, 383(2008) 78-85

[11] Chaubet, D.; Bacroix, B. and Bechade, J.L.; An EBSD Study of Static Recrystallization of cold-rolled Zircalloy-4 sheets, Materials Science Forum Vols. 408-412 (2002) 797-802

[12] Escobedo, J.P.; Cerreta, E.K.; Trujillo, C.P.; Martinez, D.T.; Lebensohn, R.A.; Webster, V.A.; Gray III, G.T.; Influence of tecture and test velocity on the dynamic, high-strain, tensile behavior of zirconium; Acta Materialia 60 (2012) 4379 - 4392

[13] Wilkinson, Angus J.; Meaden, Graham; Dingley, David J.; Mapping strains at the nanoscale using electron back scatter diffraction; Superlattices and Microstructures 45 (2009) 285-294.

[14] ASTM standard C1161-02C

[15] ASME Section III class 1

[16] INL/MIS-10-19844 Light Water Reactor Sustainability Program Quality Assurance Program Description Document

[17] LWP-1201, “Document Change Configuration Management”

[18] LWP-9201

[19] MCP-2875 Proper service and Maintenance of Laboratory Notebooks

[20] Wilkinson, Angus J.; Britton, T. Ben.; Strains, planes, and EBSD in materials science, materials Today, September 2012, Volume 15, Number 9, pp. 366-376

[21] FEI OMNI software version 5.31

[22]Buehler sample preparation technique brochure Buehler SumMet Zr Method

[23] Hovington, P.; Pinard, P.T.; Lagace, M.; Rodrigue, L.; Gauvin, R.; Trudeau, M.L.; Towards a more comprehensive microstructural analysis of Zr-2.5Nb pressure tubing using image analysis and electron backscattered diffraction (EBSD); Journal of Nuclear Materials 393 (2009) 162-174

Appendix A
An Example of the Characterization Routing Card Used for the Execution of Characterization of the Mock-up Samples on the Actual LWRS Generic Activity Sheet

LWRS Generic Activity Sheet

Requested By: Isabella VanRooyen
Completed By: _____
Project: LWRS
Date: Jan 10, 2013

Material ID#: SiC-5 **Material Description:** Zircalloy tube; the portion of the tube that was not in the HNCF basket
Material ID#: _____ **Material Description:** _____

- Note the balance calibration information if applicable

Balance Calibration #	In Calibration: ☐	Daily Check: ☐

SiC-5-1
1 (Base (no heat treatment)) 2 SiC-5-2 3 SiC-5-3 4 SiC-5-4

Process Description:

Amber, Todd 1) Cut 3/4 - 1" lengths from the tube and label (total 4)
Arnie 2) Heat treat under low O_2 - Argon atmosphere (total 3)
Todd 3) Mount + polish for EBSD
Tammy. 4) Perform EBSD

Notes:

Heat treatment:

Condition	Time	temp	Samples
a)	7 hours	450°C	2, 3
b) total of 100 hrs	100 hrs	300°C	*3, 4

* note sample 3 will be held @ 300°C for 93 hrs to get a total of 100 hrs.

- **Properly bag, label, and stow material as applicable**

Appendix B
List of Relevant Laboratory Notebooks Used for Recording of the Characterization Data

Laboratory note book number	Owner	Purpose of laboratory notebook	Relevant page numbers if applicable
LAB-E-101	Isabella van Rooyen	Relevant to all characterization and initially technology development notes	Total book
Lab note book 1834	Tammy Trowbridge	Bend test specifically and other characterization notes as needed	Total book

Note: relevant data are summarized electronically and added in the LWRS characterization drive with Isabella van Rooyen, Tammy Trowbridge and Amber Miller having “read and write” access.

Appendix C
Three-dimensional Computed Tomography X-ray imaging system

NSI-CT X-Ray Imaging System

- System Components
  - Hamamatsu 130kV Microfocus X-Ray Source
  - PaxScan 2520V Flat Panel Digital X-Ray Detector
  - Rotate Stage
  - Digital Imaging Work Station
  - Computed Tomography Work Station
- System Capabilities
  - 2D Film Radiography
  - 2D Digital Radiography (DR)
  - 2D DR with Magnification
  - 3D Computed Tomography (CT)
- Future Upgrades
  - 7-Axis Manipulator
  - 225kV X-Ray Generator

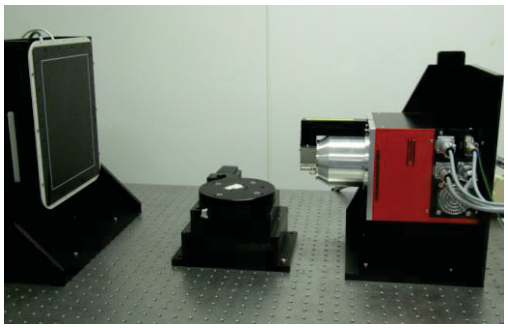

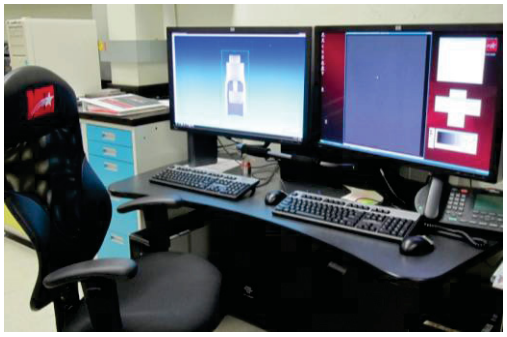

The 3D Computed Tomography X-ray imaging system at the INL Research Center was designed by North Star Imaging of Rogers, MN. Possibly the most important components of the system are the extremely powerful graphical processing unit housed in the image reconstruction computer and the proprietary image processing software.

Additional system components consist of a Hamamatsu 130kVp microfocus x-ray unit capable of producing approximately 10µm resolution images, a Varian PaxScan flat panel digital x-ray detector, and a rotational stage.

Appendix D
Timeline and Sample Preparation History

11/05/2012	SiC-1	Red Mount ①, 4 h no image	
Time delta due to Δ Resource Availability			
12/03/2012	SiC-6-1 SiC-6-2	Red Mount ①, 4 h, no patterns Red Mount ①, 4 h, etch and redo, very weak patterns	
Time delta due to Δ Heat treatment = unknown status of material; 01/10/2013 = want to verify EBSD patterns on stress relieved material Δ Christmas curtailment Δ Recourse Availability Δ Doubt in resource mind that possible in spite of literature			
01/22/2013	5-1 5-4	White mount ①	-to reduce charging x collection
01/31/2013	5-4-1	Black mount ①	Full data set not good quality
02/01/2013	5-4-2	Black mount ①	Additional vibro polish 20 h full data set, average quality
02/07/2013	5-1 5-1-1	Black Mount ② Black Mount ②	4 h vibro partial data set Additional vibro partial data set
02/08/2013	5-1-2	Black Mount ②	Additional vibro full set, bad quality
02/12/2013	5-1-3	Black Mount ②	New Buehler polish 4 h vibro, full final set, average quality
02/15/2013	SiC-6-10	Black Mount ②	4 h bad quality
	SiC-6-11 SiC-6-12	Black Mount ②	12 h, EBSD parameters slightly better film surface
02/16/2013	SiC-1-10	Black Mount ②	12 h poor results
02/18/2013	SiC-1-11	Black Mount ②	13 h vibratory check results on 02/19/2013, average results
02/19/2013	SiC-2	Will do overnight 02/19/2013	
02/20/2013		Will have one average set of each bend test sample.	

Appendix E
Electro polishing detail of samples LWRS-1-A-6-1

Zr-based samples for metallographic and EBSD analysis were cut and mounted in phenolic resin to yield mounts with a nominal diameter of 25.4 mm. The mounts were then ground and polished. The final polishing step utilized 0.3 μm alumina slurry to produce a mirror finish. The samples were then electropolished using a Struers LectroPol-5. The electrolyte was methanol-36% 2-butoxyethanol-5% perchloric acid. Electropolishing was carried out at 17˚C and 24 volts for approximately 5 seconds to remove surface deformation caused by mechanical grinding and polishing without producing significant surface topography that could interfere with EBSD analysis.

Appendix F
Buehler SumMet methods used for samples SiC-5-1, SiC-1, SiC-2 and SiC-6

Copied from Buehler SumMet Methods

Table 17. Four-Step Procedure for Zirconium and Hafnium

Surface	Abrasive/ Size	Load Lb. (N)/ Specimen	Base Speed (rpm)/Direction	Time (min:sec)
CarbiMet 2 abrasive discs (waterproof paper)	320- (P400) grit SiC water cooled	5 (22)	200-250 Comp.	Until Plane
UltraPol or UltraPad cloths	9-µm MetaDi Supreme diamond suspension*	5 (22)	150-200 Contra	5:00
TriDent cloth	3-µm MetaDi Supreme diamond suspension*	5 (22)	150-200 Contra	3:00
MicroCloth, VelTex or ChemoMet cloths	~0.05-µm MasterMet colloidal silica plus attack polish agent**	6 (27)	120-150 Contra	7:00

*Plus MetaDi fluid extender as desired **See text for agent
Comp. – Complementary (platen and specimen holder both rotate in the same direction
Contra – Platen and specimen holder rotate in opposite directions

** I used 2 parts 30% Hydrogen peroxide to 8 parts MasterMet Colloidial silica for the attack polish

Zirconium and Hafnium
Pure zirconium and pure hafnium are soft, ductile hexagonal close-packed metals that can deform by mechanical twinning if handled aggressively in sectioning and grinding. As with most refractory metals, grinding and polishing removal rates are low and eliminating all polishing scratches and deformation can be difficult. It may even be possible to form mechanical twins in compression mounting. Both can contain very hard phases that make relief control more difficult. To improve polarized light response, it is common practice to chemically polish specimens after mechanical polishing. Alternatively, attack polishing additions can be made to the final polishing abrasive slurry, or vibratory polishing may be employed. Table 17 is a four-step procedure that can be followed by either chemical polishing or vibratory polishing. Several attack polishing agents have been used for Zr and Hf. One is a mixture of 1-2 parts hydrogen peroxide (30% concentration – avoid all skin contact) to 8 or 9 parts colloidal silica. Another is 5 mL of a chromium trioxide solution (20 g CrO_3 to 100 mL water) added to 95 mL colloidal silica or MasterpPrep alumina slurry. Additions of oxalic, hydrofluoric or nitric acids have also been used. All of these attack polishing additions must be handled with care as they are strong oxidizers. Skin contact must be avoided. Chemical polishing solutions are reviewed in [2]. Cain's has been popular. Use under a hood and avoid skin contact. Ann Kelly developed an excellent chemical polish for refractory metals, such as Zr, Hf, and Ta. It consists of 25 mL lactic acid, 15 mL nitric acid and 5 mL hydrofluoric acid. Swab vigorously for up to 2 minutes. To prepare ultra-pure Zr and Hf, the above method is unsatisfactory and a procedure, such as in Table 15 (add a 5- or 3-µm alumina step) is needed, as diamond is ineffective. Use the chromium trioxide attack polish with the alumina and conclude with Kelly's chemical polish.

Appendix G
Grain Size Distribution

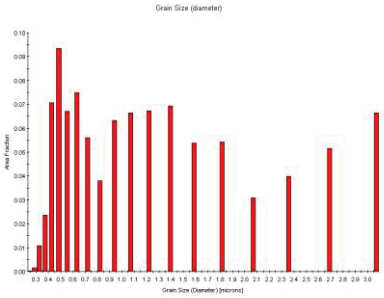

SiC 1-11

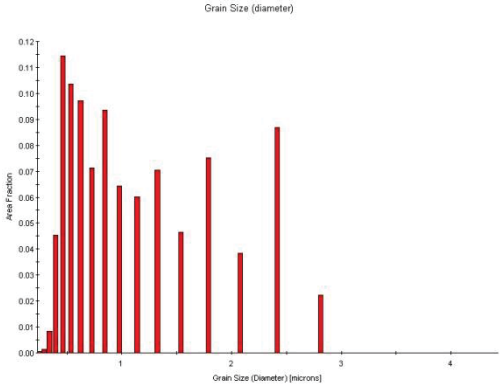

SiC 2-10

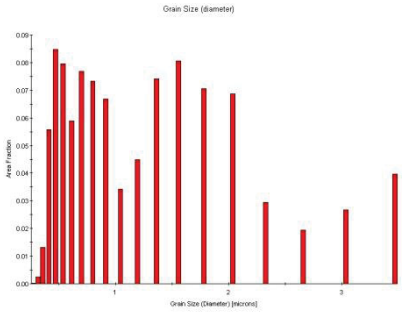

SiC 6-10

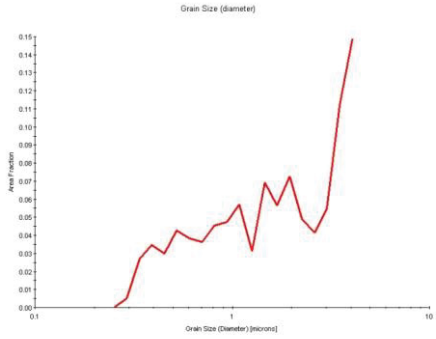

5-4-2

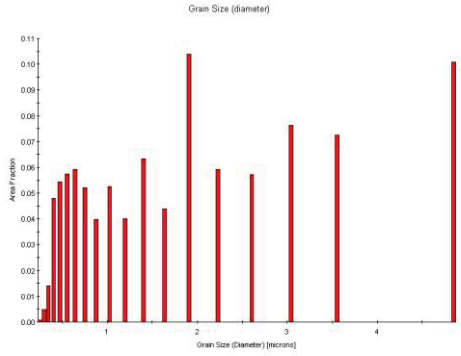

5-1-3

Appendix H
Misorientation Angles: Rough Data

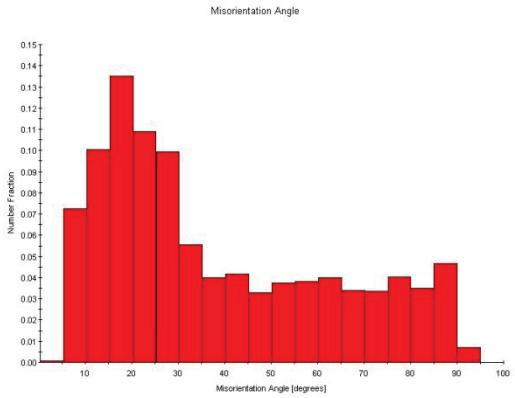

SiC-5-1-3

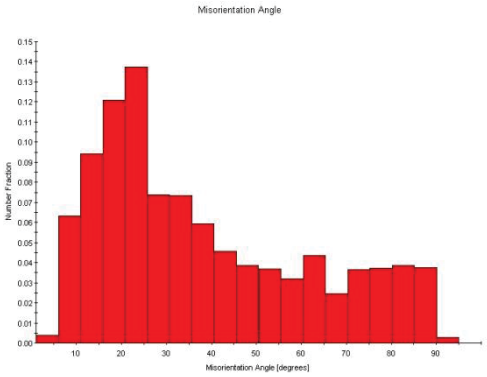

SiC-5-4-2

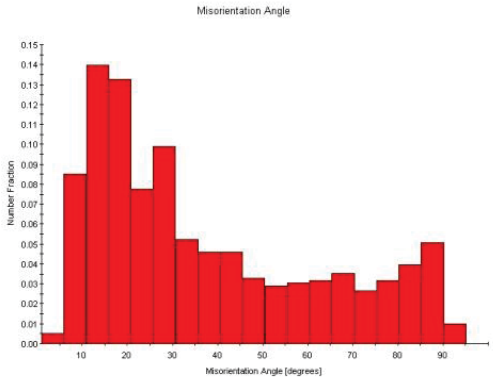

SiC-1-11

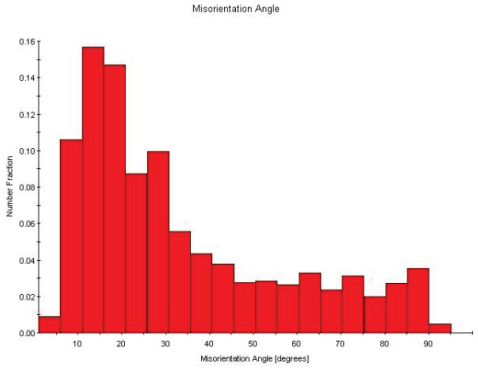

SiC-2-10

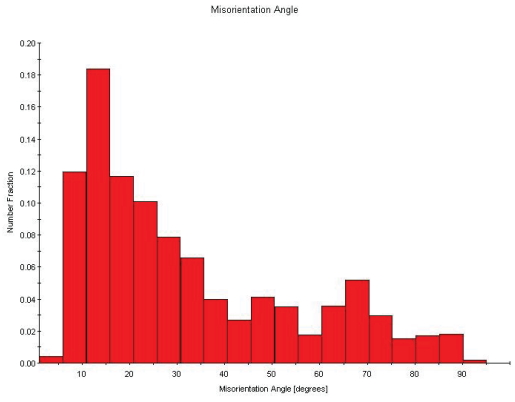

SiC-6-10

Appendix I
Grain Boundary Character Distribution

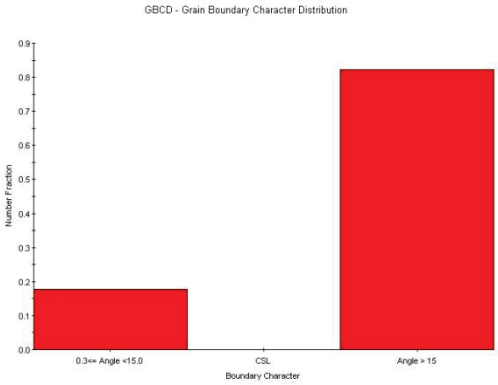

SiC-5-1-3

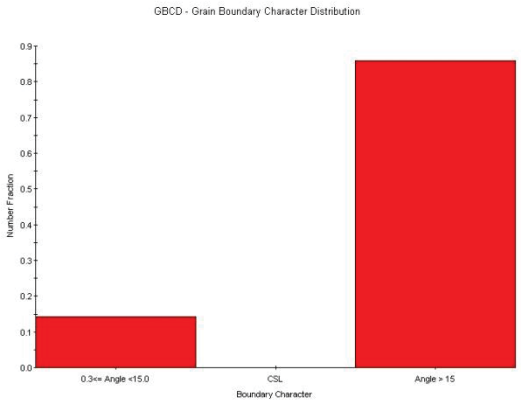

SiC-5-4-2

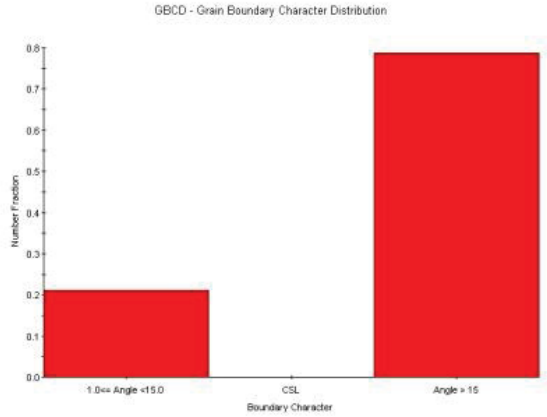

SiC-1-11

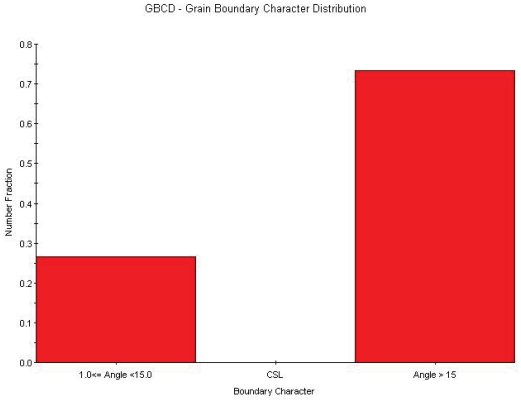

SiC-2-10

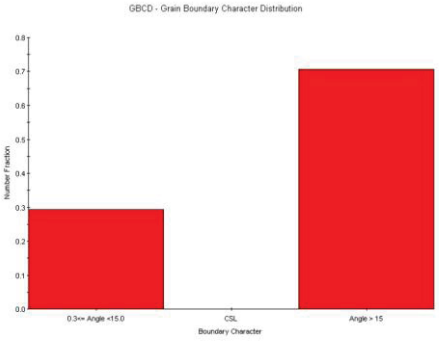

SiC-6-10